Morino Lecture 2015

Molecular Rotation Signals: Molecule Chemistry … and Particle Physics

Jens-Uwe Grabow

Institut für Physikalische Chemie & Elektrochemie, Lehrgebiet A,
Gottfried-Wilhelm-Leibniz-Universität, Callinstraße 3A
30167 Hannover, République Fédérale d'Allemagne;
E-mail: jens-uwe.grabow@pci.uni-hannover.de

Molecules - large or small - are attractive academic resources, with numerous questions on their chemical behaviour as well as problems in fundamental physics now (or still) waiting to be answered: Targeted by high-resolution spectroscopy, a rotating molecular top can turn into a laboratory for molecule chemistry or a laboratory for particle physics.

Once successfully entrained (many species - depending on size and chemical composition - have insufficient vapour pressures or are of transient nature, such that specifically designed pulsed-jet sources are required for their transfer into the gas phase or in-situ generation) into the collision-free environment of a supersonic-jet expansion, each molecular top comes with its own set of challenges, theoretically and experimentally: Multiple internal interactions are causing complicated energy level schemes and the resulting spectra will be rather difficult to predict theoretically. Experimentally, these spectra are difficult to assess and assign. With today's broad-banded chirped-microwave techniques, finding and identifying such spectral features have lost their major drawback of being very time consuming for many molecules. For other molecules, the unrivalled resolution and sensitivity of the narrow-banded techniques provide a window to tackle - at the highest precision available to date – fundamental questions in physics, even particle physics – potentially beyond the standard model.

Molecular charge distribution, properties of the chemical bond, details on internal dynamics and intermolecular interaction, the (stereo-chemical) molecular structure (including the possibility of their spatial separation) as well as potential evidence for tiny yet significant interactions encode their signature in pure molecular rotation subjected to time-domain microwave spectroscopic techniques. Ongoing exciting technical developments promise rapid progress. We present recent examples from Hannover, new directions, and an outlook at the future of molecular rotation spectroscopy.

Molecular Rotation Signals: Molecule Chemistry … and Particle Physics

Jens-Uwe Grabow*[1]

Molecules - large or small - are attractive academic resources, with numerous questions on their chemical behaviour as well as problems in fundamental physics now (or still) waiting to be answered: Targeted by high-resolution spectroscopy, a rotating molecular top can turn into a laboratory for molecule chemistry or a laboratory for particle physics.

Once successfully entrained (many species - depending on size and chemical composition - have insufficient vapour pressures or are of transient nature, such that specifically designed pulsed-jet sources are required for their transfer into the gas phase or in-situ generation) into the collision-free environment of a supersonic-jet expansion, each molecular top comes with its own set of challenges, theoretically and experimentally: Multiple internal interactions are causing complicated energy level schemes and the resulting spectra will be rather difficult to predict theoretically. Experimentally, these spectra are difficult to assess and assign. With today's broad-banded chirped-microwave techniques, finding and identifying such spectral features have lost their major drawback of being very time consuming for many molecules. For other molecules, the unrivalled resolution and sensitivity of the narrow-banded techniques provide a window to tackle - at the highest precision available to date – fundamental questions in physics, even particle physics – potentially beyond the standard model.

Molecular charge distribution, properties of the chemical bond, details on internal dynamics and intermolecular interaction, the (stereo-chemical) molecular structure (including the possibility of their spatial separation) as well as potential evidence for tiny yet significant interactions encode their signature in pure molecular rotation subjected to time-domain microwave spectroscopic techniques. Ongoing exciting technical developments promise rapid progress. We present recent examples from Hannover, new directions, and an outlook at the future of molecular rotation spectroscopy.

Keywords : microwave spectroscopy, rotational spectroscopy, coherence spectroscopy, time-domain, Fourier transform, double resonance.

Introduction:

A large variety of techniques have been developed to record spectra that are associated with transitions between rotational states. For most molecules and molecular systems these transitions occur in the microwave (MW) region, Table I. While molecular rotation spectra traditionally are associated with molecular structure determination, today's microwave spectroscopy is addressing a wide variety of basic and applied key-problems in Physical Chemistry, Molecular Physics, and related fields: Questions on molecular structure, conformational and tautomeric conversion, chemical bond, charge transfer, and internal dynamics of are elucidated not only for isolated molecules. In the spectral signature of rotating molecules one might even search for effects, which could answer fundamental questions in particle physics.

While the mm wave and sub-mm wave ranges of high-resolution microwave spectroscopy are still dominated by frequency domain techniques, the cm wave range has been taken over by time domain techniques. We shall discuss most of the basic modern methods that use microwave oscillators as coherent light sources as well as some more specialized ones that use arbitrary waveform generation to overcome specific problems and open a wide field of new opportunities.

Experimental Methods:

Microwave Spectroscopy Techniques: In traditional microwave spectrometers monochromatic radiation is passed through a sample cell and the transmitted signal is detected [1]. Due to the presence of a sample the radiation is modified. To yield the spectrum the signal is recorded as a function of the incident radiation frequency. The majority of recent frequency domain spectroscopy (FDS) instruments are using backward wave oscillators (BWO) as continuous wave (CW) swept frequency sources that can cover a broad frequency region.

Instead of continuously passing monochromatic radiation through a sample cell and detecting the transmitted signal as a function of frequency, contemporary microwave spectrometers

[1] Gottfried-Wilhelm-Leibniz-Universität, Institut für Physikalische Chemie & Elektrochemie, Lehrgebiet A, Callinstraße 3A, 30167 Hannover, République Fédéral d'Allemagne. – mail: jens-uwe.grabow@pci.uni-hannover.de; phone: +49(511)762-3163, fax: +49(511)762-4009.

apply the radiation for short period of time [2,3]. In the presence of a sample a radiative response is induced. To yield the spectrum the response signal is recorded as a function of time and subjected to Fourier-transformation (FT). The trend in microwave spectroscopy toward more sophisticated experiments such as time domain spectroscopy (TDS) instruments was initiated by the aim to detect the rotational spectra of ions or short-living reaction products and thus the development of more sensitive detection systems became mandatory.

Pulsed Radiation Fourier-transform Microwave Spectroscopy: The time-dependent behavior of absorption and emission of two-level quantum mechanical systems enables the possibility of the measurement of rotational transitions in the time-domain, analogous to the pioneering development of pulsed nuclear magnetic resonance (NMR) experiments. Microwave-molecule resonant transient phenomena are centered on two main processes: *transient absorption*, which is normally called transient nutation (TN) in NMR experiments, and *transient emission*, which is normally called the free-induction decay (FID) in NMR experiments. Transient experiments in NMR have been familiar for two decades before their routine introduction in MW spectroscopy in 1974. Normally, the relaxation times in magnetic resonance experiments are 10^6-10^7 times longer than in gas-phase rotational systems. Thus, the radiation switching and speed of detection requirements in rotational state spectroscopy are much more severe, and this has led, in part, to the long delay in developing transient experiments in rotational spectroscopy. The transient signal is recorded as the beat between the radiation field coherently emitted from the molecular system and the signal of the microwave oscillator used for polarization. The signal obtained is subsequently Fourier-transformed to give the spectrum of the transitions which were polarized. In comparison to absorption methods Fourier transform microwave (FT-MW) techniques offers the same advantages as experienced in FT-NMR.

The magnitude of the macroscopic oscillating dipole moment, i.e., the sample polarization and thus the amplitude of the corresponding microwave field emitted at the end of a MW pulse depends on the coupling strength of the molecular dipoles with the external radiation [4]. For a transition b←a with the electric dipole matrix element μ_{ab} of the space-fixed ***z***-component of the dipole operator, this coupling strength is characterized by the Rabi angular frequency $x = \mu_{ab}\, \varepsilon / \hbar$, where ε is the z-polarized electric field amplitude of the external radiation. The polarization achieved depends on x, the MW pulse length τ_p, and the offset $\Delta\omega = \omega_{ab} - \omega_e$ from resonance. Effects from collisional damping and deviations from resonance during the pulse can be neglected for strong pulses ($x >> \Delta\omega$) sufficiently short with respect to the relaxation times ($\tau_p << T_2$). For the period after the transient absorption, the amplitude $|S_{ab}|$ of the molecular signal after super-heterodyne detection is proportional to

$$|S_{ab}| \propto \Delta^1 N_{ab} \mu_{ab} \sin(x\tau_p) \exp(-t/T_2) \qquad (1)$$

where $\Delta^1 N_{ab}$ is the population difference per unit volume of the two levels involved in the transition. According to Eq. (1), the largest signal amplitude S_{ab} is obtained for a '$\pi/2$-pulse', defined by a pulse angle $x\tau_p = \pi/2$. The exponential decay of the transient emission time-domain signal due to collision-induced relaxation corresponds to a pressure broadening of the frequency-domain line with a half width at half mean (HWHM) of $\Delta\nu_{ab} = 1/2\pi T_2$. At low pressures other broadening mechanisms than intermolecular collisions become important and the decay term in Eq. (1) has to be modified accordingly. As seen below, the sensitivity of FT-MW spectroscopy is inherently larger, such that quite low sample pressures can often be used and pressure broadening becomes rather unimportant. Due to the lack of modulation and saturation broadening occurring in absorption techniques, the resolution is then only limited by Doppler- and wall collision broadening, which depend on the frequency range and cell geometry, respectively [5]. The enhanced resolution of FT-MW spectroscopy translates into a higher precision of observed line center frequencies.

The TDS technique is inherently more sensitive than the FDS methods, i.e., the initial transient emission signal amplitude after a '$\pi/2$-pulse' is larger than any steady-state absorption signal [6]. The sensitivity enhancement is particularly pronounced for conditions $S_p = xT_2 >> 1$, ensuring that an '$\pi/2$-pulse' ($x\,\tau_p = \pi/2$, $\tau_p << T_2$) converts the initial population difference ΔN_{ab} efficiently into coherence ρ_{ab}. Comparing the resulting signal amplitude S_{ab}(TDS) of the FT technique with the signal amplitude S_{ab}(FDS) corresponding to the steady-state polarization [4], applicable to the CW absorption method, yields

$$S_{ab}(\mathrm{TDS}) / S_{ab}(\mathrm{FDS}) = (1 + S_p^2) / S_p \qquad (2)$$

if identical detection schemes, e.g. super-heterodyne detection, are employed in both experiments. As a consequence, at $S_p >> 1$, low gas pressures can be employed and, if the incident MW power is sufficiently high, transitions with rather weak dipole matrix elements can still be investigated [7]. The linear signal dependence upon the dipole matrix element μ_{ab} in FT-MW spectroscopy evident differs from the quadratic μ_{ab}^2 dependence obtained for CW absorption spectroscopy at low MW power. For the latter method, this means a severe disadvantage in sensitivity for small transition dipole moments [8].

Covering the frequency range from 1 – 40 GHz various cm wave range pulsed power designs of static gas FT-MW spectrometers are employing coaxial (1 – 4 GHz) and rectangular or circular (4 – 40 GHz) waveguides [7-10]. A mm wave range implementation follows the frequency switching technique [11]. At such shorter wavelength free-space sample cells can also be used.

Pulsed Radiation FT-MW Double-Resonance Experiments: In extension to single resonance methods, double resonance (DR) techniques were already introduced in the early

period of impulse FT-MW spectroscopy on static gases. Such experiments were first only employed to facilitate an easy assignment of rotational transitions by simplifying the one-dimensional (1D) spectra. DR methods applying CW radiation for a second resonance were soon extended to experiments based on excitation pulse trains for both 'signal' and 'pump' resonance frequencies [12]. Further developments of pulsed DR techniques allow the simultaneous determination of both resonance frequencies by employing two-dimensional (2D) spectra [13]. A variety of pulse sequences have been created for quite different applications. Among the variety of 2D FT-MW DR techniques, the 'double-quantum' (DQ) correlation sequence is the most important so far. Since it retains the sensitivity at the 'signal' transition, it allows for highly sensitive experiments employing 'pump' frequencies which are significantly lower than the 'signal' frequency. Accordingly, after its original development for MW-DR spectroscopy, this method was extended to RF-DR spectroscopy being based on a 'pump'-transition in the RF range [14] such that pure nuclear quadrupole hfs transitions can be observed [15].

Supersonic-jet Fourier-transform Microwave Experiments: If molecular species are prepared in the velocity-equilibrating conditions of a supersonic-jet expansion, Doppler- and collision-induced broadening become rather unimportant. Consequently, FT-MW spectroscopy on pulsed supersonic-jet expansions has become popular due to their unique ability to provide high resolution and high sensitivity simultaneously. In the course of the supersonic-jet expansion, converting the enthalpy of the sample set by thermal equilibrium conditions before the expansion into directed translational energy, also weakly bound species are formed. Once existing, these species are isolated in the collisionless environment of the expanding gas and hence persist however weak the binding. In the advent of the technique, after being specifically developed as a method of investigating the rotational spectra of weakly bound molecular complexes [16], studies on such systems have dominated the application of the method.

After the early reports on FT-MW spectroscopy on pulsed supersonic-jet expansions [17], a number of significant advances in the technique were achieved especially in recent years [18-23]. Presently, this MW spectroscopic method serves as one of the most productive techniques and shall be presented in detail. The state-of-the-art supersonic-jet expansion resonator FT-MW spectrometer discussed here provides further improvements in some significant points [24]. The general design considerations on its high-frequency electronics are generally instructive for all FT-MW methods however. This implementation is especially suited for the detection and characterization of larger, instable compounds – also in very small concentrations. A block diagram of the spectrometer, using a short MW radiation pulse for excitation, is presented in Fig. 1; its components are: (1) MW wobble generator, 10 dBm output power; (2) MW SPDT switch, 50 dB isolation, 3 dB insertion loss; (3) MW SSB modulator, 15 dB carrier suppression, 12 dB insertion loss; (4) MW variable attenuator, 0…71 dB attenuation; (5) MW coaxial cable, flexible; (6) MW power amplifier, 25 dB gain, 13 dBm output power; (7) MW directional coupler, 20 dB coupling, 1.2 dB insertion loss; (8) MW power sensor, 20…-70 dBm input power; (9) MW electro-mechanical switch, 60 dB isolation, 1.25 dB insertion loss; (10) MW termination, 50 Ω impedance; (11) MW low-noise amplifier, 1.1/2.0 dB noise figure at 77/300 K, 30 dB gain, 0 dBm output power; (12) MW diode detector, 0.5 mV/μW sensitivity; (13) MW IR demodulator, 18 dB image rejection, 14.5 dB insertion loss; (14) RF low-noise amplifier, 1.2 dB noise figure, 35 dB gain, 6 dBm output power; (15) RF bandpass filter, 2.0 MHz 3dB-bandwidth, 2dB insertion loss; (16) RF VGC amplifier, -13…17dB gain, 3 dB output power; (17) RF signal generator, 10 dBm output power. (18) RF I/Q demodulator, 7 dB insertion loss; (19) RF lowpass filter, 6 MHz 3dB-bandwidth; (20) PXI-based experiment control, data-acquisition, and –analysis system; (21) frequency standard, 10 MHz output frequency; 10^{-11} frequency accuracy; (22) RF distribution amplifier, 13dBm output power; (23) RF frequency doubler, 0dB gain; (24) RF frequency tripler, 0 dB gain; (25) RF QPSK modulator, 4x 90°; (26) RF VGC amplifier, -6…24dB gain, 13 dB output power; (27) RF GaAs SPDT switch, 40 dB isolation, 0.9 dB insertion loss; (28) RF termination, 50 Ω impedance. In avoiding components which operate only in octave bands or otherwise limited in their bandwidth, e.g., waveguides, isolators, circulators, power divider, etc.., a very broadband instrument can be constructed such that – without any modifications – multi-octave operation from 2 – 26.5 GHz is possible [22]. All essential external spectrometer components are integrated into the experiment control, data-acquisition, and –analysis system either using the general-purpuse-interface-bus (GPIB) or local-area-network (LAN), all internal components are using the PCI-eXtensions-for-Instrumentation (PXI). While using the platform-independent virtual-instruments-software-architecture (VISA) and interchangeable-virtual-instruments (IVI) drivers, the entire spectrometer can be controlled via a graphical user interface (GUI) operated either interactively or completely automated [21].

The electric dipole interaction of the molecular sample, discussed with the optical Bloch equations describing the time-evolution of a two-level system in resonance or near resonance with the external field, is based on the exposition to a standing wave field of the microwave radiation propagating in a TEM_{plq}-mode of a Fabry-Pérot type resonator. It's geometric and electric parameters have a profound impact on the sensitivity of the spectrometer, especially at the low-frequency end. While cylindrical cavity designs utilizing the low-loss TE_{01}-mode have also been tried [25], considerable improvements were achieved in optimizing parameters of the resonator. Rather extreme geometries have been utilized [26]. Also operation throughout the mm wave range was sought [27]. Further developments include cryogenic operation of the resonator spectrometer [23]. The resonator arrangement discussed here provides advantages in some significant points [24]. It is also suited for sensitive detections in the lower frequency range important for the study of bigger or heavier species, i.e. molecular systems exhibiting larger moments of inertia.

The use of an electromagnetic valve does not only reduce the gas load to the pump system, such that its required capacity is reduced; it can also ideally be combined with the pulse excitation scheme of the FT-MW TDS technique. Skimming or collimation of the expansion

to achive a narower line width leads to serious intensity losses for the observed signals [28]. In contrast to this and in comparison to a gas mixture that is introduced perpendicularly to the resonator axis, the resolution as well as the sensitivity of the supersonic-jet expansion FT-MW spectroscopy in Fabry-Pérot-type resonators could be significantly increased with the introduction of the ‚coaxially-oriented-beam-resonator-arrangement' (COBRA) [19, 22]. The set-up given in Fig. 2 exhibits a jet source in the center of one of the reflectors which form the resonator.

The diluted gas mixture - typically $\leq 1\%$ in a rare gas at a total pressure in the range 50 – 500 kPa – is expanded into the evacuated resonator chamber. The nozzle, in its simplest form, consists of a 2mm long conus that increases from 0.5 – 2.0 mm diameter to 4 mm diameter. The properties of the gas expansion are of qualitative as well as quantitative importance for the rotational spectrum of molecular system under investigation, i.e. the effective translational, rotational, and vibrational temperatur of the species, as well as the spatial distribution and the chemical nature of the systems present in the jet.

The flow of the gas which expands through the nozzle into the evacuated resonator chamber, is supersonic rather than effusive: Resulting from the sudden adiabatic expansion, the molecular systems exhibit a very small effective rotational and usually a significantly reduced vibrational temperature. Eventually, they are moving in a collision-free expansion at velocity v on radial trajectories. Before the expansion, the gas assumes a Maxwell-Boltzmann distribution at tht molecular velocity v_0 which is defined by its temperatur T_0 at thermal equillibrium. After the adiabatic expansion, we have a highly directed mass flow: Binary collisions at the early stages of the expansion lead to a transformation of the undirected motion of all species to a directed translation. The internal energy of the molecular species is transfered to directed kinetic energy. Accordingly, the rotational and vibrationl energy of the expanding molecules drops rapidly while the Maxwell-Boltzmann velocity distribution narrows and, at the same time, shifts from its starting value a v_0 very close to ist limit v_∞:

$$v_\infty = (2k_B T_0/m \times \gamma/\gamma\text{-}1)^{1/2} \quad , \quad \gamma = c_p/c_v \tag{3}$$

with the heat capacities of the gas mixtures at constant pressure and volume c_p and c_v, respectively, the Boltzmann constant k_B, and the mean mass of all species m. Effectively, this corresponds to a complete transformation of the enthalpy in directed kinetic energie for $T_0 >> T_t \approx 0$ K, with the translational temperature T_t assuming the value of the terminal velocity distribution. In very good approximation, the properties of the expansion is, at vast excess, determined by the rare gas. For a diluted mixture, m and γ can therefor be fixed at the rare gas values. The translational temperature of the supersonically expanded rare gas can be calculated [29]. At the conditions described here, translational temperatures of $T_t < 1$ K are predicted. The resulting narrowed velocity distribution corresponds to such small relative velocities, that the molecules, once leaving the region of high number density, effectively move collision-free. Because of the still large number of collisions when the gas is just exiting the nozzle channel, also very low rotational temperatures are expected, since a high efficiency is assumed for rotation-translation energy transfer. The vibrational temperatures of species in the supersonic jet are higher but also quite low. Without special measures, such as, e.g., in a plasma generation, rotational transitions have only be observed in a few cases at - and then only in low-lying – vibrationally excited states.

The spatial distribution of the molecules exiting the jet source is well described by a mass flow, in which all molecules move with the same velocity v_∞ along radial trajectories at an angle θ with respect to the symmetry axis [24]. At time t, limited by the spatial extension of the supersonic jet generated at a pulse length τ_M, the molecular number density ${}^1N(\mathbf{r},t)$ at distance r from the jet souce becomes

$${}^1N(\mathbf{r},t) = (b+1)N/2\pi v_\infty \tau_M \times \cos^b(\theta)/r^2 \tag{4}$$

where the coefficient b can vary from 1 to 3 for an ideally effusive and an ideally supersonic expansion, respectively; the total number N of the species in the jet is experimentally determined by the consumption of the known gas mixture or, if the sample, e.g., is generated in-situ, of by suitable diagnostic methods. With Eq. (4) it becomes obvious that due to the enhancement factor $\kappa_p = (b+1)/2$ the near-axis number density – in the COBRA set-up coinciding with the active region of the resonator – is increased by a factor of two for supersonic jets compared to effusive expansions.

The interaction of the microwave radiation and the molecular systems within the supersonic-jet expansion results in rotational coherence which establishes a polarized sample moving coaxially along the resonator axis. While the exciting MW field is relatively short-lived, the polarization of the molecular ensemble, due to the collisionless environment, is persistent Fabry-Pérot type. The time-evolution is discussed with the optical Bloch equations describing of a two-level system in absence of an external field. With very long relaxation times T_2 collisional broadening does not need to be considered. Instead, the expansion of the jet on the radial trajectories, thus reducing the number density of the molecular ensemble contributing to the molecular field in the resonator, is becoming the dominant mechanism for the decay of the signal. The lineshape due to the time-dependent number densities according to is still close to a Lorentzian in the frequency domain after FT. The molecular signal power as a function of time is finally obtained as that fraction of the total energy, stored by the field over the resonator volume, which is lost due to coupling to the receiving electronics of the spectrometer [23]. The amplitude $|S_{ab}|$ of the molecular signal after super-heterodyne detection is proportional to:

$$|S_{ab}| \propto Q_L^{1/2}\, \Delta N_{ab}\, \mu_{ab}\, sin(x\tau_p)\, cos(kv_\infty t) \quad (5)$$

where $Q_L = \omega/\delta\omega$ is the loaded Quality factor of the resonator having a spectral mode width $\delta\omega$, ΔN_{ab} represents the two-level population difference of the total number of species in the jet and $k = \omega/c$ is the wavenumber of the radiation. During to the transient emission, the spatial distribution of the jet expanding along the resonator axis is projected on the TEM_{plq} mode fulfilling the resonance condition for propagation in the Fabry-Pérot resonator. As a result of the jet expanding with a terminal velocity v_∞ along the resonator axis, the molecular field is modulated in time as given in Eq. (3), resulting in

$$S_{ab}(t) \propto s' exp(i((\omega_{ab}-kv_\infty)t+\theta'_{ab})) + s'' exp(i(\omega_{ab}+kv_\infty)t+\theta''_{ab})) \quad (6)$$

and thus a Doppler doublet consisting of frequency components at $v_{ab}(1 - v_\infty/c)$ and $v_{ab}(1 + v_\infty/c)$ is observed in the frequency domain. The molecular resonance frequency is then recovered as the arithmetic mean of the components separated by $\Delta v_{ab} = 2v_{ab}v_\infty/c$. The linewidth (HWHM) of the individual components is on the order of *1.5 kHz*, or *0.0000005* cm^{-1}; at an appreciable S/N ratio a frequency accuracy of *150 Hz*, or *0.00000005* cm^{-1} is achieved for unblended lines. This extraordinary resolution provides supersonic-jet expansion FT-MW spectroscopy with a chemical specific unrivalled by any analytical method [30].

Zero-field Molecular Characterisation: Owing the sensitivity low-abundant, transient, or otherwise experimentally challenging species can be studied, in particular because supersonic-jet expansions are combined with, e.g., heated, LASER-ablation- [31,32], DC-discharge-plasma sources [23,33,34], or even a combination of the latter two[35]. Thus, many larger organic or inorganic species that have low vapour pressures or are unstable at normal conditions can to be transformed into the gas phase by thermal [36, 37, 38, 39, 40] or radiative heating [41-45, 46, 47, 48, 49] or are generated in-situ [50,51], respectively. Also excimer-LASER are used for in-situ generation of transient species from precursors entering the Fabry-Pérot type resonator [42]. In another approach, valves equipped with flow- [43,44] and mixing- [45] assemblies can be employed to supply instable species. Further studies include the initial phase of solvation processes [46]. One of the key-capabilities of supersonic FT-MW spectroscopy is the precise characterization of intra-molecular tunneling processes [44,47-60]. The method is successful in the structural determination of conformational preferences in chiral molecules [61] as well as the characterization of van-der-Waals internuclear potentials in diatomics[62], aggregation of larger rare clusters [63] and effects of quantum salvation[64]. The rotational spectra of species that are thermally, e.g. due to intra-molecular elimination reactions [52], easily affected, can be accessed by ultra-fast evaporation using ps-LASER. Also excimer-LASER are used for in-situ generation of transient species from precursors entering the Fabry-Pérot type resonator [53]. In another approach, valves equipped with flow- [54,55] and mixing- [56] assemblies can be employed to supply instable species.

Today's work is rotational spectroscopy include the study of inter-molecular hydrogen bonds of different nature [57, 58, 59] and the initial phase of solvation processes [60]. One of the key-capabilities of supersonic FT-MW spectroscopy is the precise characterization of intra-molecular tunneling processes [55,61-71] , which can be of multi-dimensional nature [72, 73, 74, 75]. It can also be studied, if intra-molecular tunneling barriers are introduced sterically or electronically [76, 77, 78].

The method is successful in the structural determination of conformational preferences in chiral [79, 80] and bio-molecules [52, 81, 82, 83], as well as physiologically or pharmacologically active molecules [84, 85]. Polymorph systems, such as, e.g., sugars, notorically give problems in their structural characterisation: Even if diffraction methods are applicable, the structure is affected by cristal lattice forces and therefor can deviate from the equilibrium structure of the isolated molecule. Methods of NMR in condensed phases result in solvent-averaged indirect structures [86, 87, 88]. Structural informationen of chromophor-marked systems can be gained from ultraviolet-ultraviolet (UV-UV) and infrared-ultraviolet (IR-UV) double-resonance techniques in LASER-spektroscopic experiments [89]. Here, however, LASER-spectroscopy obtains only vibrational resolution, such that the band assignment is not always unambiguous. Conversely, pure rotational spectroscopy does not require a chromophor, at the same time delivering unrivalled resolution. Rotamers, conformers and isomers as well as isotopologs are unambiguously identified as independent species via their moments of inertia with respect to quantum-chemical prerdictions; Fig. 3 demonstrates this showing a section a rotational spectrum obtained from D-ribose: Aldopentoses like ribose can assume a lineare form or exist in two cyclic forms: 5-membered rings (furanose, Fur) or 6-membered rings (pyranose, Pyr), which occur, depending on the orientation of the hydroxyl group at the C_1 position, either as α- or β-anomer. In standart textbooks, ribose is usually depicted as β-furanose, the predominant form in ribo-nucleosides, ARN, ATP and other bio-chemical relevant derivatives. Furanose and pyranose rings exhibit further conformational variations: Pyranose assumes a $^1C_4$ or $^4C_1$ conformation, which can be transformed into each other by ring inversion. Boat structures of ribo-pyranose are, while less probable, also plausible. Furanoses can change between different envelope forms like C_2-*endo* or C_3-*endo* via non-planar structures. Finally, the different hydroxyl-groups can give rise for a multitude of rotamers. Here, cooperative hydrogen bonds are observed: In the experimentally determined global minimum $^1C_4$, the hydroxyl-groups of the carbon atoms 2-4 form a network of three intra-molecular hydrogen bridges as depicted in Fig. 4 (bond distances from supporting MP2-calculations, ring-conformation as well as axial (Ax)/equatorial (Eq) hydroxyl-orientation result in three different lengths of the hydrogen bridges). The cooperative networks can be clockwise (c) or counter-clockwise (cc). As the most stable forms of D-Ribose not β-Furanose but conformers of β-Pyranose were found: cc-β-Pyr $^1C_4$, energetically followed by cc-β-Pyr $^4C_1$ [52].

The best available equilibrium structurs are obtained from a semi-experimental ansatz of microwave spectra in combination with quantum-chemical calculations [90, 91]. Of important theoretical impact is finally also the experimental characterization of van-der-Waals internuclear potentials in diatomics [92], aggregation of larger rare gas clusters [93] and effects of quantum solvation [94].

Supersonic-jet FT-MW Stark-effect Experiments: Despite of all differences in the various FT-MW techniques, the accuracy of Stark effect measurements was always limited by the inhomogeneity of the employed electric field. Since the supersonic-jet expansion, as well as the MW electric field propagating in a low-loss TEM_{plq} mode of the Fabry-Pérot resonator, requires a substantially larger free volume than a static gas in a waveguide experiment, the impact of field inhomogeneities becomes more severe however. Conventionally, Fabry-Pérot resonator spectrometers for the measurement of the Stark effect employ a pair of high-voltage electrodes that consist of rectangular or quadratic plates or nets facing each other perpendicularly to the resonator axis [95]. Several approaches to increase the field inhomogeneity were followed: Obviously, a more homogeneous field can be achieved in changing the ratio of the electrodes dimensions with respect to their distance [96]. However, the choice of electrode distance and extension is limited by the propagation of the MW radiation if the sensitivity of the spectrometer has to be maintained. This is especially important in the lower frequency range, since the MW field distribution is significantly widened towards larger wavelength. Another approach employs an array of wires running parallel to the edges of the electrodes. The wires - connected in series by resistors acting as potential dividers - homogenize the electric field at the outer regions of the plate electrodes [97]. Such wires can only be placed parallel to the edges above and below the resonator axis. Also additional sheets of metal placed at the edges of the plates can increase the homogeneous region of the electric field between the Stark electrodes [98].

A very homogeneous electric field can be obtained with the reflectors of the Fabry-Pérot resonator itself serving as Stark electrodes after being mounted electrically insulated. Thus, the rear reflector can be set to a high electric potential of up to $U_z = 20$ *kV*, while the front reflector, equipped with the MW antennae and the jet source, has to be kept at ground potential. As illustrated in Fig. 5, the reflectors alone are not producing a sufficiently homogeneous electric field. However, in employing additional coaxial ring electrodes, i.e. the utilizing the 'coaxially aligned electrodes for Stark-effect applied in resonators' (CAESAR) arrangement [99], the field is homogenized very effectively. In this arrangement, the ring electrodes and the reflectors are connected via identical resistors. Guided by numerical simulations, the distances of the identical ring electrodes with a diameter matching the reflector's diameter, are adjusted such that a constant potential gradient along the resonator axis is produced. The resulting electric field is homogeneous over a large volume. Inhomogeneities in radial directions occur sufficiently far away from the resonator axis and thus, as a consequence of the Gaussian TEM_{plq} modes confining the active volume of the resonator around its axis, the inhomogeneous regions practically do not contribute to the observed molecular signal. The CAESAR setup thus provides the principle advantages of a COBRA spectrometer for Stark effect experiments, such that the exceptionally sharp signals enable a very precise determination of dipole moments [100, 101, 102]. Since the direction of the static electromagnetic field is parallel to the resonator axis and thus perpendicular to the MW field vector, the transitions obey the selection rule $\Delta M = 1$.

Due to the enlarged sensitivity and increased resolution, narrow spectral splittings of shifts cannot only be observed for species at low concentrations or with small dipole moments, respectively; also the characterization of larger, polycyclic aromatic molecules, e.g. compounds of astrochemical importance [36, 37, 38, 39]. Here, fundamental questions on the nature and constituents of the interstellar medium and circumstellar envelopes arise as fascinating junction of astronomy, spectroscopy, and chemistry. The combination of high performance laboratory spectroscopy with high performance radio astronomy open new vistas to detect and identify molecular key-species in the interstellar medium (ISM). At the begin of this decade, 151 compounds, 125 isotopologs and 2 conformers were known to exist in the interstellar medium, most of them from radio astronomy. Eight additional species were found in comets. However, detection by radio astronomy is not feasible for unpolar or only weakly polar species, since the microwave signal is quadratically dependent on the molecular dipole moment. Even though numerous (polar) carbon-rich molecules exist in space, simple aromatic, polycyclic aromatic hydrocarbons (PAH), and fullerenes turned out to be rather unaccessible by radioastronomy. Molecular infrared emissions are observed in a variety of astronomical sources, but IR emission data are naturally less precise than the highly resolved microwave spectra obtained from radio astronomy. Therefor the spectroscopic detection of aromates and PAHs (with the possible exceptons benzene, $C_{60/70}$) remains ambiguous and these species thus represent eminently important targets for the verification and modelling of the known or predicted chemistry of the interstellar molecular clouds and circumstellar gas envelopes. Here, corannulene assumes a special key-position: Corannulene, contrary to the most (planar) polycyclic aromatic hydrocarbons, which only exhibit a small or – at given symmetry – even no dipole moment. is not planar, see Fig. 6, due to its structural strain. The strain-induced pyramidization of the central carbon atoms of corannulene results, as predicted by quantum-chemical MP2 calculations [103], in a quite substancial dipole moment. The detection of ist rotational spectrum as that of an exceptionally rigid symmetric rotor with five-fold rotational symmetry and subsequently lifting the M-degeneracy, Fig. 7, by the Stark effect according to $H_E = -\boldsymbol{\mu} \cdot \boldsymbol{E}$ enables the experimental determination of its dipole moment $\mu = 6.908(60)\ 10^{-30}$ Cm (2.07 D) [36]. Indeed, this is the largest value of a pure hydrocarbon measured to date, making corannulene a sensitive key-species for the still missing radioastronomical detection of a PAH.

Supersonic-jet FT-MW Zeeman-effect Experiments: For molecular systems in a $^1\Sigma$ state, magnetic fields on the order of 1 T are typically necessary, to observe a Zeeman-effekt.

Species with electronic contributions to the angular momentum exhibit significantly larger magnetic moments, which depend on the orbit angular momentum $\boldsymbol{L}$ and the spin $\boldsymbol{S}$ of unpaired electrons:

$$\boldsymbol{\mu}_L = \mu_B \boldsymbol{L} \quad , \quad \boldsymbol{\mu}_S = -g_e \mu_B \boldsymbol{S} \tag{7}$$

where μ_B is the Bohr magneton and $g_e = 2\mu_e/\mu_B = 2.0023$ is the g-factor of the free electron. Typically, the Zeeman-effekt according to $H_B = -\boldsymbol{\mu} \cdot \boldsymbol{B}$ of species with unpaired electrons is four orders of magnitude more sensitive to magnetic fields than the sensitivity of closed-shell molecules. Therefor, observable spectral splittings are already induced by the Earth's magnetis field.

While the Zeeman-effect provides valuable information on the electronic structure of molecula systems, it often might still be desirable to avoid the Zeeman-effekt when studying species with unpaired electrons. By suppressing the Zeeman-splitting, not only the analysis of complicated spectra, which still exhibit an additional hyperfine splitting due to spin coupling, is eased. More important – if unknown species in low concentrations are searched for - is the lower detection limit due to the increased intensity of the unsplit transitions. To eliminate the Earth's magnetic field, so-called Helmholtz coils can be employed. An arrangement of three pairs of Helmholtz-coils, shown in Fig. 8, enables the compensation of all spatial components. The magnetic flux-density $\boldsymbol{B} = \mu_r\mu_0\boldsymbol{H}$, which is caused by a pair of coils rings with large diameters at an electric current I, is fairly homogenious is their distance d equals their radius R. Along the **y**-coils axis, the magnetic field strength of **y**-directed field **H** amounts to

$$H = IR^2/2 \quad (1/(R^2+(d/2 - y)^2)^{3/2} \quad + \quad 1/(R^2+(d/2 + y)^2)^{3/2}) \tag{8}$$

while a similar dependence exists in the radial direction. If such a coil arrangement is employed in combination with a Fabry-Pérot-Type resonator, a sufficiently homogeneous field is obtained at a coil pair distance, that, at least, corresponds to the distance of the resonator reflectors. Then, the line-width of the COBRA spectrometer is also preserved for zero-field experiments on species with ungepaired electrons, such that – at exceptionally sharp signals – their very precise characterisation succeeds. Starting from the compensated Earth's magnetic field, the currents of a coil pair can be lowered, to adjust for defined magnetic fields parallel or perpendicular to the microwave field for Zeeman-experiments; the selection rules $\Delta M = 0$ and $\Delta M = 1$, respectively, are set by the direction that was chosen. Because of the very narrow signals, the Zeeman-Effekt is precisely measured also at the small fields **B** that can be achieved, such that a very accurate determination of molecular g-factors is possible.

This way, the exceptionally accurate characterisation of – for a potential measurement of the postulated electron electric dipole moment (e-EDM) very interesting – lead fluoride, PbF, in the $^2\Pi_{1/2}$ state succeeded**:** Fundamental symmetry leads to an ±M-degeneracy of any molecule or atom, which is preserved even at the presence of an E-field along the quantisation axis. The existance of an e-EDM, however, would break this symmetry. An e-EDM therefor leads to an energy difference $\boldsymbol{\Delta U} = U_{+M} - U_{-M}$ in a strong E-field parallel and anti-parallel to a B-field. At the current experimental upper e-EDM limit $d_e \leq 0.9 \times 10^{-28}$ e cm [104], atomic spectroscopy requires extremely high external E-fields for a measurable effect. But the effect can be searched for by molekalar spectroscopy: In diatomic systems with heavy nuclei, e.g. PbF, unpaired electrons, due to relatistic orbit effects, the so-called Lorentz contraction, experience an effective internal E-field. If the diatomic molecule also exhibits (systematic or random) near-degenerate states with opposite parity, complete polarisisation of the system can already be obtained with moderate E-fields. Therefor, with the random near-degeneracies of hyperfine levels found in $^{207}Pb^{19}F$, shown in Fig. 9, huge internal effective fields of ~60 GV/cm can be achieved at external fields of only 200V/cm. The diatomic compound is synthesized in-situ by LASER-ablation [105] from a rotating elementary Pb-rod at presence of highly dilluted SF_6 in Ne as carrier. Field-free transitions (and later also their Zeeman-splittings) of the species $^{206}Pb^{19}F$, $^{207}Pb^{19}F$, and $^{208}Pb^{19}F$ can be recorded in natural abundance at an absolute accuracy of a fraction of a kHz within seconds [106] – at a linewidth, that approximatele corresponds to those, that where reported for e-EDM sensitive experimenty on YbF [107]. The precision of the $^{207}Pb^{19}F$ spectra reached – without special measures – the necessary sensitivity to observe the extremely small Ω-doublett dependence on the nucleus-rotation-interaction; the projection quantun number $\Omega = \Lambda + \Sigma$ gives the total projection of the electron spin and electronic angular momentum on the molecular axis. The accuracy of these measurements in comparison to presious spectroscopic studies on this molecule is impressively demonstrated in Fig. 10. Standard FT-MW spectroscopy, as shown here in comparison to other techniques, approaches the level of accuracy, required to detect parity(P)-violating effects in experiments adapted for this task. While a rotational spectrocopy detection of the - also P-violating – so-called anapol-interaction, which relies on the penetration of a nucleus by unpaired s-elektrons, is within immediate reach, the detection of an e-EDM will require a leap in accuracy which might be achived by utilizing a combination of special techniques – e.g. recording the rotation of the planar polarization as the science signal.

Chirped Radiation Fourier-transform Microwave Spectroscopy:

The TDS technique has the further advantage over FDS steady-state techniques, that the time required to record a spectrum in the transient excitation experiment is *a-priori* independent of the width of the spectrum. In principle, this 'multiplex advantage' translates to an improvement of the S/N ratio in a spectral band which is proportional to the square root of the spectral band to the linewidth ratio [9]. However, unlike in pulsed NMR spectroscopy

[108], this S/N improvement was, until recently, not exploited in FT-MW spectroscopy, in particular for high-Q resonator techniques or in the case of low transition dipole moments for waveguide methods, because of the rather limited excitation bandwidth obtained so far, if excitation is achieved by 'short exposure' (SE) to a stationary frequency radiation field.

If the frequency of an electromagnetic field is swept through a molecular resonance in a time short compared to the relaxation time, so-called 'fast passage' (FP) excitation occurs. Even though the molecules are in resonance only for a very short time, a surprisingly large change in the population difference of the states in resonance and coherence of the two-level ensemble can be achieved, resulting in an appreciable oscillating macroscopic polarization. FP can thus be rationalized as transient absorption during the sweep followed by transient emission after the sweep [109]. Comparing the resulting signal amplitude S_{ab}(FP) of the frequency ramp technique with the signal amplitude S_{ab}(SE) obtainable by the resonant stationary frequency ($x >> \Delta\omega$) method at a given geometry of a sample cell with flat frequency response, yields

$$S_{ab}(FP) / S_{ab}(SE) = x\,(2\pi/\alpha)^{1/2} / \sin(x\tau_p) \qquad (9)$$

with the Rabi angular frequency $x = \mu_{ab}\,\varepsilon / \hbar$ of the transition b←a characterized by the electric dipole matrix element μ_{ab}, the duration τ_p of the resonant radiation pulse, and the slope $\alpha = d(\Delta\omega)/dt$ of the frequency ramp of a z-polarized electric field ω_e with the amplitude ε at offset $\Delta\omega = \omega_{ab} - \omega_e$ from resonance ω_{ab}. With $x^2/\alpha << 2\pi$ a *linear* FP according to $x/2\pi << \alpha / x = d(\theta(\Delta\omega))/dt$ has been assumed, i.e., in the Bloch vector model the precession frequency is low compared to changes $d(\theta(\Delta\omega))/dt$ in the direction of its precession axis [6]. This is consistent with negligible population excitation $d(\Delta N_{ab})/dt \approx 0$. It becomes clear from the Boch vector model, that for $x/2\pi \approx \alpha / x$, i.e. the precession frequency is similar to the reorientation $d(\theta(\Delta\omega))/dt$ of the precession axis upon FP, also a population equilibration $\Delta N_{ab} \approx 0$ can be obtained. Any molecular transition b←a in the band passed by the frequency ramp $\omega_i \leq \omega_e(t) \leq \omega_f$ will be polarized:

Fig. 11 shows the result for a frequency ramp on the example of difluorophenol [110]. The comparison with an a-priori prediction of this part of the rotational spectrum by MP2 calculations demonstrates the importance of the IMPACT methods – as described in the following section - for a fast visual assignment of spectral signatures by broadband pattern recognition. While the ratio S_{ab}(FP) / S_{ab}(SE) of a single experiment is typically an order of magnitude smaller than one, the bandwidth $\omega_f - \omega_i$ of the frequency rampe, also known als ‚chirp', can be several orders of magnitude wider than the Fourier-limited spectral coverage of a stationary frequency ‚pulse'.

In-Phase/Quadrature-Phase-Modulation Passage-Acquired-Coherence Technique: Even though - since resonators of high quality can not be utilized - more experiment repetitions become necessary, to maintain the S/N ratio of the SE method in FP experiments, often the 'multiplex advantage' still enables a large improvement in the S/N-ratio for a spectral band that has to be recorded in limited time. Exploitation of the multiplex advantage in early attempts of the FP experiment [109, 111, 112] was limited in the slope and coverage of the frequency ramp, which needed to be supplied at sufficient phase stability for coherent experiment repetitions, as well as by the lack of performance in the high-speed signal acquisition and by the huge signal processing.

With the enormous advances in digital electronics one can now create phase coherent broadband MW frequency ramps as well as achieve sufficiently fast digitization and massive signal processing. The sensitivity and extreme broadband capabilities of the method are impressive [113]. Even though the specifications of key-components required for FP experiments are quite demanding, the instrumental effort can significantly be reduced for 'very' rather than 'ultra' broadband operation [114]. The state-of-the-art supersonic-jet expansion FP FT-MW spectrometer discussed here provides advantages in some significant points [115, 116]. The general design considerations on its high-frequency electronics are generally instructive for all FP methods [117]. Utilizing the intriguingly elegant in-phase/quadrature-phase (I/Q) modulation scheme for direct single-sideband frequency translation, the design implements the 'in-phase/quadrature-phase-modulation passage-acquired-coherence technique' (IMPACT). This implementation, with readily available components allowing for frequencies from 2.0 - 26.5 GHz in a single setup, is especially suited for the detection and characterization of larger, instable compounds – also in very small concentrations. A block diagram of the IMPACT spectrometer, using a short MW radiation frequency ramp for excitation, is presented in Fig. 12; the components of the - compared to other FT-MW instruments - relatively simple set-up are: (1) MW signal generator, 10 dBm output power; (2) MW SPDT switch, 50 dB isolation, 3 dB insertion loss; (3) RF arbitrary-signal generator, 2x 1.25 Gs/s generation,, 15 bit resolution: (4) MW I/Q-upconverter, 15 dB carrier suppression, 12 dB insertion loss; (5) MW coaxial cable, flexible; (6) MW (very-)high-power amplifier, >27 dB gain, >30 dBm output power; (7) MW termination, 50 Ω impedance; (8) MW horn antenna w/ offset-parabola reflector, 25 dBi gain; (9) MW low-noise amplifier, 2.8 dB noise figure, 30 dB gain, 0 dBm output power; (10) MW I/Q-downconverter, 18 dB image rejection, 14.5 dB insertion loss; (11) MW lowpass filter, DC-990 HMz, 2dB insertion loss; (12) MW Digitizer, 2x 2 GS/s real-time acquisition; (13) PXIe-based experiment control, data-acquisition, and –analysis system; (14) Rubidium-Frequency Standard, 10 MHz Output Frequency, $5x10^{-10}$ frequency stability. The relative arrangement of molecular jet and high-frequency field is very similar to a semi-confocal COBRA apparatus but with parabolic reflectors not forming a resonator. The polarization of the velocity-equilibrated molecular jet - expanding coaxially with respect to the high-frequency incident and reflected radiation beam, as demonstrated in Fig. 13 [110] – also causes a Doppler doublet with its components exhibiting only a very small spectral width on the order of the COBRA experiment (FWHH ≅ 3 kHz) since the observation time is

similar in this arrangement. At good signal-to-noise ratio the signal frequency can then be determined as accurate as 300 Hz or 0.00000001 cm^{-1}.

Thus, the IMPACT-apparatus is not only suitable for rotational spectroscopic first-time assignment of a molecule, also the high-resolution analysis succeeds using the same spectra that are acquired routinely. For difluoro phenol [110], the energy difference ΔE = 8.47399(22) MHz as well as the Coriolis-coupling parameters between the v = 0 symmetry species of the intra-molecular tunneling motion of the hydroxyl-H atom could therefor be directly determined from the fine structure of the broadband spectrum. Thus, the IMPACT spectrometer combines the spectral overview of the broadband free-space instruments with chirp-excitation for fast collection and eased assigment of spectra with the unrivalled high resolution of the narrow-banded resonator set-ups with pulse-excitation for the precise analysis even of subtile effects.

WIDE-IMPACT FT-MW Technique: Using the IMPACT set-up described above, the real-time bandwidth of the method is still not completely exploited, such that another enhancement of the multiplex advantage will immediately reduce even further the time-effort required for the acquisition of overvioew spectra [118]. This becomes especially valuable, if the predictive power even of expensive quantum-chemical calculations is only sufficient, to guess the position of spectrale signatures, but not to localize them with certainty. The identification of the water-hexamer $(H_2O)_6$ is an exceptional example [119]. The true potential of this experimetal development effort however, as shown below, is not the fast acquisition of plain oiverview spectra.

The state-of-the-art supersonic-jet expansion wide-band FP FT-MW spectrometer discussed here maintains the IMPACT advantages while extended frequency coverage for single experiments is achieved [115, 110]. The general design considerations on its high-frequency electronics provide further opportunities for additional, more complex experiments [117]. This implementation is especially suited for the detection – also in very small concentrations – and characterization of compounds exhibiting dynamical processes. A block diagram of the WIDE-IMPACT spectrometer, using a short MW radiation frequency ramp for excitation, is presented in Fig. 14. By wide-band I/Q-modulation it is feasible to generate another impulse or CW signal without delay after FP excitation. Thus 2D or 1D, respectively, FP FT-MW MW-DR experiments are inherently possible where conventional spectrometers would need an additional coherent source. Since I/Q-modulators for extreme frequency coverage are lacking commercial availability, wide-band I/Q-modulation has to be realized using discrete components making the basic block diagram look more complicated while really it is not. Unlike other FT-MW spectrometers the WIDE-IMPACT apparatus does not even require a tuneable MW source; the particular implementation utilizes a fixed-frequency dual-sideband source assembly thereby doubling the frequency coverage. The components of the MW-DR capable FP set-up are: (1) MW phase-locked oscillator, f_0, +12 dBm; (2) MW phase-locked oscillator, f_1, +12 dBm; (3) arbitrary-waveform generator, 2x DC... f_1; (4) digital oscilloscope, 2x DC... $2f_1$, real-time acquisition; (5) PXIe-based experiment control, data-acquisition, and –analysis system; (6) distribution amplifier, 5x 10MHz; (7) frequency standard, 10MHz, $5x10^{-10}$; (8) MW SPDT-switch, f_0-f_1...f_0+f_1, speed: 20ns, insertion loss < 3.0 dB; (9) MW termination, f_0-$2f_1$...f_0+$2f_1$; (10) MW modulator, IF-in: f_1, LO-in: f_0, RF-out: f_0-f_1...f_0+f_1; (11) MW modulator, IF-in: DC... f_1, LO-in: f_0-f_1...f_0+f_1, RF-out: f_0-$2f_1$...f_0+$2f_1$; (12) MW modulator, RF-in: f_0-$2f_1$...f_0+$2f_1$, LO-in: f_0, IF-out: DC... $2f_1$; (13) MW driver amplifier, Freq: f_0-f_1...f_0+f_1, +20 dBm, 27 dB; (14) MW in-phase power divider/combiner, 0°/0°, f_0-$2f_1$...f_0+$2f_1$; (15) MW bandpass filter, f_0-f_1, insertion loss: <1.0 dB, rejection: 30 dB; (16) MW bandpass filter, f_0+f_1, insertion loss: <1.0 dB, rejection: 30 dB; (17) MW quadrature-phase power divider, 0°/90°, f_0-f_1; (18) MW quadrature-phase power divider, 0°/90°, f_0+f_1; (19) MW quadrature-phase power divider, 0°/90°, f_0; (20) MW lowpass Filter, DC... $2f_1$, insertion loss: <0.5 dB, rejection: 30 dB; (21) MW pre amplifier, f_0-$2f_1$...18GHz, 22 dBm, 29 dB; (22) MW pulsed high-power amplifier, f_0-$2f_1$...18GHz, 63 dBm, 46 dB; (23) MW power amplifier, f_0-$2f_1$...f_0+$2f_1$, 27 dBm, 27 dB; (24) MW high-power limiter, f_0-$2f_1$...18GHz, 1.5 kW, insertion loss: < 3.0 dB; (25) MW horn antenna w/ offset-parabola reflector, f_0-$2f_1$...f_0+$2f_1$, 25 dBi; (26) MW low-noise amplifier, f_0-$2f_1$...f_0+$2f_1$, noise figure: < 3.0 dB, 27 dB; (27) MW SPDT-switch, f_0-$2f_1$...f_0+$2f_1$, speed: 20ns, insertion ioss < 3.0 dB; (28) MW directional coupler, < -10 dB, f_0; (29) MW in-phase power divider/combiner, 0°/0°, f_0-f_1...f_0+f_1.

In exploiting the frequency agility of the I/Q-modulation setup 2D or 1D FP FT-MW MW-DR experiments are easily performed with a single MW source. Since the WIDE-IMPACT apparatus provides wide-band coverage in single experiments, 2D FT-MW MW-DR experiment sequences with wide-band coverage in both dimensions now become time-efficient and thus feasible while conventional supersonic-jet expansion COBRA FT-MW spectroscopy can still be performed in the entire instrumental range by employing a Fabry-Pérot type resonator instead of a sample cell or a free-space interaction assembly with flat frequency response.

Chirped Radiation FT-MW Multi-Resonance Experiments: The FP technique can easily be combined with additional static or oscillating external fields as demonstrated above for the established FT-MW methods. Also in this realm, the broad frequency coverage provides intriguing advantages. When applying static fields, e.g. Stark-effect measurements, precise frequency shifts are obtained for a large number of transitions at once, providing a ‘multiplex advantage’ of a different kind: Instead of precisely determining the Stark-effect for a molecular system on a limited number of lines for various electric fields, the frequency shifts of many lines measured at once can be evaluated for a single electric field.

Even more promising are the DR capabilities of the FP technique arising from the ‘multiplex advantage’. Due to drastically reduced time-effort for wide frequency coverage in the MW domain, 2D DR spectroscopy, which required an unrealistic time budged if broad coverage in both domains was desired, is now becoming feasible for many frequency regions in the

second domain. In principle, the FP technique can be combined with DR excitation from almost any frequency region of the electromagnetic spectrum exploiting the extended capabilities that arise from the fast production of broad 1D or 2D spectra. Arbitrary waveform generation of the MW frequency ramp and direct I/Q-modulation, in avoiding subsequent mixing and multiplication stages, allows for exact signal shaping in amplitude and phase. Thus cm wave DR excitation sequences at almost any complexity can easily be generated and provide the possibility for DR experiments being even more elaborate than the sequences presented for FT-MW with stationary gases. Additional mm wave and sub-mm wave DR sources can now probe connectivity of resonances in MW spectra in a broadband fashion. For IR DR interaction the typical bandwidth of an IR-LASER pulse is broad enough to excite multiple quantum states. Thus, FP FT-MW IR-DR spectra are not quantum-state resolved. To obtain state resolved spectra an FP FT-MW MW/IR-TR experiment can be employed [120].

The state selection can be based on radiative coupling of levels, which can be set to any part of the MW region, by utilizing either the cm wave impulse capabilities of the FP FT-MW setup or an additional mm wave or sub-mm wave source. 2D-spectra can then be obtained in two different ways, i.e. the second dimension of the spectra can span across different domains: By active scanning of the IR-LASER wavelength, 2D MW/IR spectra are generated; by incrementing the (MW,mm,sub-mm)-source frequency, 2D MW/(MW,mm,sub-mm) spectra are generated. A supersonic-jet setup for FP FT-MW detected (MW,mm,sub-mm)/tunable-IR triple-resonance interaction is depicted in Fig. 15: Via a periscope (2) the tunable mid-IR radiation (1) of a pulse-Nd:YAG-LASER pumped ‚optical-parametric-oscillator/optical-parametric-amplifier' (OPO/OPA) LASER-system is directed into a multipass setup (3) of two concentric spherical reflectors of high reflectivity, having the radiation passways cross the jet's expansion volume. For an efficient overlap, a slit-nozzle (4) instead of a circular orifice can be utilized. The mm wave or sub-mm wave signal (5) is based on a primary cm wave generator, multiplied by an active mm oder sub-mm wave module and phase-locked to the frequency standard of the FP FT-MW instrument shown in Fig. 14, wich polarizes (7a) and detects (7b) the molecular probe via the horn antenna/reflector-setup. If the primary generator - internally or externally – allows for it and also the subsequent signal modules are compatible with an I/Q- or phase-modulation, complicated coherence-experiments become possible. The horn antenna (6) irradiates the expanding jet with the elektromagnetic field.

Conclusion: The development of A/D- and D/A-converters is one of the most dynamic fields of technical development, resulting in new devices such as the fast A/D-recorder and D/A-sources which are expected to outdate the still widely used analog sources and signal-processing devices. Considering the versatility combined with even wider coverage and higher frequencies soon to be reached, it is anticipated that FP FT-MW implementations like, e.g., WIDE-IMPACT discussed above are becoming the most interesting instruments for FT-MW spectroscopy and will revolutionize the field.

Without chromophore, single rotamers, conformers and isomers as well as isotopologs can be unambiguously identified simultaneously as free species at highest resolution in a short time; Fig. 16 demonstrates this with a section of the rotational spectrum obtained from Vitamic C (mp = 190°C), which required a recording time of 75 minutes instead of >1 day in a conventional measurement: Vitamin C is a γ-lactone ring, wich exhibits two hydroxyl groups and an ethyldiol side-chain. The four hydroxyl groups can simultaneously act as proton-donor and/or –acceptor, the keton- and ether-groups function as proton acceptor. With 5 internal degrees of freedom to conformerization, 11 intra-molecular hydrogen bonds become accessable, which can form three different types of bonds: O-H...O=C, O-H...O und O-H...O-H. This bridge puzzle can stabilize numerous energetically low-lying conformers. In fact, MP2/6-311++G(d,p) ab-initio calculations predict up to 17 conformers within 900 cm^{-1} (nine conformers within 700 cm^{-1}, Fig. 17), which exhibit up to four simultaneous intra-molecular hydrogen bonds. The spectral transitions can unambiguously assigned to exactly three rotamers I, II und III forming the hydrogen bond networks (1,3,6,8), (1,5,7) bzw. (12,4,7). Likely due to this complexity, no gasphase experiments on vitamin C have been reported before – in addition, the high melting point (190°C) and thus low vapor pressure make the experiment even more difficult. To date, gasphase experiments on any vitamins where limited to photo-elektron spectroscopy of the vitamins A [121] and D [122]. The required combination of FP FT-MW spectroscopy with LASER-ablation – while utilizing the third harmonic (λ=355nm) of a ps-LASER - for a fragmentation-free evaporation of vitamin C [123] opens a wide vista for the razor-sharp characterization of larger, delicate bio-organic molekules.

The most exciting perspective for FP FT-MW might be its suitability for rotational spectroscopy directed towards the observation of dynamic processes: Since the dynamical behavior manifests itself in the overall spectral envelope, the foremost prerequisite for such measurements is the fast wide-band coverage at reliable reproduction of line intensities ideally without sacrificing the sensitivity of narrow-band FT-MW methods. This allows for a paradigm shift in MW spectroscopy: Being well established in determining the geometrical and electronic structure of molecular systems, including various effects of non-rigidity, the field focused on problems that did not require a time-dependent treatment as mostly ground-state or only moderately vibrationally excited systems are accessible in conventional spectrometers. Now the preparation of excited molecules by LASER excitation opens up new vistas on dynamical effects to be elucidated by MW spectroscopy, exploiting its unrivaled resolving power and high sensitivity, e.g., the kinetics of conformational isomerization [120]. Furthermore, it is expected that the LASER-excitation schemes for dynamic spectroscopy probed by FP FT-MW multi-resonance techniques can be expanded to higher energy regions from the IR to the UV, then accessing dynamics above the barrier to isomerization.

This is possible because of the Hamiltonian remaining bound, i.e. the isomerization of the molecular systems is still characterized by stationare wavefunctions with corresponding

discrete energy levels. Even though the transformation between individual species of different shape requires a time-dependend treatment, they are still characterized by rotational frequencies, which can be based on the different moments of inertia of the participating structures. Different from other spectroscopic methods, a direct link between the spectral position of an observed signals and the entire structure of the molecular carrier is established, which then leads to an unambiguous assignment. Finally, it can be expected, that LASER-excitation schemes for dynamical spectrocopy - detected by FP FT-MW multi-resonance techniques – will be extended to higher energy regions from IR to UV, such than the dynamic beyond the barrier to isomerisiezation become accessible.

Figure Captions:

Figure 1. Supersonic-jet expansion COBRA FT-MW spectrometer: Records of *~1 MHz* spectral width within *2.0-26.5 GHz* frequency range.

Figure 2. Supersonic-jet expansion Fabry-Pérot-type resonator chamber: (1) aluminum reflectors (green), $\sigma = 1.6 \times 10^7$ 1/Ωm conductivity, $a' = 315$ mm radius, $b' = 630$ mm radius of curvature, $d = 530...730$ mm distance; (2) linear translation stage, 100 mm extension, 0.5 µm resolution, 25 mm/s speed; (3) stainless steel six-way cross DN630 ISO-K, 1033 mm diameter, spherical center-body; (4) oil diffusion pump DN630 ISO-F, 20000 L/s pump capacity; (5) roots blower/2-stage-rotary vane pumpstand, 210/65 m^3/h pump capacity. The jet-source is located in the center of the left reflector (source: Fig. 3.6 in [24])

Figure 3. Part of the COBRA FT-MW overview spectrum of D-ribose. The six detected conforms of the free ribose are pyranose 5-ringe, which assume $^1C_4$- oder $^4C_1$-chair structures. The three conformers that have quantum-chemially be predicted as lowest in energy are β anomers, the three other observed conformers are α anomers. (source: Fig. 1 in [52])

Figure 4. Cooperative intra-molecular hydrogen bond networks (quanten-chemically predicted distances in Å) of the two most stable conformers of D-ribose cc-β-Pyr $^1C_4$ and cc-β-Pyr $^4C_1$. C: blue (mit position labelling), O: red; H: grey. Clockwise (c) and counter-clockwise (cc) cooperative netzworks are distinguished. (source: Fig. 4 in [52])

Figure 5. CAESAR-FT-MW sdt-up for rotational Stark-effekt measurements. Of the two reflectors, held by insulating mounts, the right (red) can be set to a high electric potential ($|U| \leq 20$kV), while the left (green) is held at ground potential. A chain of resistors connecting coaxial ring electrodes between the reflectors homogenize the electric field E. (source: Fig. 3.13 in [24])

Figure 6. Curved structure of corannulens, $C_{20}H_{10}$. The polarity of the molecule arises from the strain-induced pyramidalization of the carbon atoms in the central 5-ring, which forces the polycyclic network into a non-planar bowl.

Figure 7. Quadratic Stark-effect of corannulene: Frequency shift of the M_J-components of the rotational transition $J_K = 6_0 - 5_0$. (source: Fig. 2 in [36])

Figure 8. COBRA FT-MW resonator chamber with Helmholtz-coils for controlled suppression of the rotational Zeeman-effect of open-shell molecular species. Three orthogonal pairs (blue) with coil distance $d=R$ snd radius R = 750mm are utilized to compensate the Earth's magnetic field or to adjust for a defined magnetic field component parallel or perpendicular to the polarization direction of the radiation field. (source: Fig. 3.15 in [24]).

Figure 9. Hyperfine levels of the two lowest-energy rotational states of $X_1(v = 0)$ $^{207}Pb^{19}F$ (right) as well as $^{206}Pb^{19}F$ and $^{208}Pb^{19}F$ (left). **F** is the total angular momentum **F = J + I** with nuclear spin **I**. p_s reflects the parity of the wavefunction. (source: Fig. 1 in [105])

Figure 10. Frequency scale for the resolved measurement of the named energy terms of lead fluoride, PbF, in comparison to the resolving capabilities of several spectroscopic methods: LASER-induced fluorescens (LIF), resonance enhanced multi-photon ionization (REMPI), pseudo-continuos(pc) REMPI and FT-MW. ***J*** is the total angular momentum, ***S*** is the electronic spin, ***I*** is the nuclear spin and ***n*** gives the inter-nuclear axis; the terms are lead by the rotational and related coupling constants, respectively: The rotational constant *B*, the fine-structure constante *p*, spinrotational coupling constant *c* and their higher order correction *d* as well as the spin-spin coupling constant t_0. The (kartesian) tensor contractions $\boldsymbol{I}\cdot\cdot\hat{A}\cdot\cdot\boldsymbol{S}$ can be written as spherical tensor contractions $A_{\|} I^1{}_0S^1{}_0 - A_{\perp} (I^1{}_1S^1{}_{-1} + I^1{}_{-1}S^1{}_1)$ with the hyperfine couplings constants $A_{\|}$ und $A_{\perp}$. *W*p and W_d are the parity-violating sensitivities of the molecule towards a nuclear anapole moment κ_p and towards a dipole moment of the electrons d_e, respectively.

Figure 11. Radiation-chirp FT-MW experiment. Top: Spectrum of a 1 GHz frequency ramp excitation of 2,6-difluorophenol. The insert shows the transient chirp-response before Fourier-transformation. Bottom: a-priori simulation of the spectrum characterized by the large-amplitude tunneling motion of the hydroxyl-group from quantum-chemical predictions. The degree of agreement between theory and experiment is sufficient for a first-time assignment of quantumnumbers to characteristic signals to initiate a quantum-mechanical analysis. (source: Fig. 3 in [110])

Figure 12. Supersonic-jet expansion IMPACT FT-MW spectrometer: Records of ~1 GHz spectral width within *2.0-26.5 GHz* frequency range.

Figure 13. IMPACT FT-MW experiment: Rotational spectrum of 2,6-difluorphenols. Left: Antenna-reflektor-nozzle-Arrangement for a quasi-coaxial propagation of supersonic-jet and elektromagnetic field. Right: Magnification of two lines, due to the coaxial configuration occuring as Doppler-douplet of very narrow components. (source: graphical abstract to [110]/titelpage of [118].

Figure 14. Supersonic-jet expansion WIDE-IMPACT FT-MW spectrometer: Records of *>10 GHz* spectral width within *6.5-26.5 GHz* frequency range.

Figure 15. Supersonic-jet expansion FP 2D FT-MW IR/mm-wave triple-resonance experiment. Components and minimum specifications are: (1) tunable mid-IR pulse-LASER source: 1350 – 5000 nm, ~10 mJ, 20 Hz, $\Delta\lambda < 0.02$ cm-1; (2) periskope; (3) Multi-pass cell; (4) pulse valve; (5) mm-wave source, 60 - 325 GHz; (6) mm wave, sub-mm wave horn-antenna, 60 – 325 GHz , > 24dBi antenna gain; (7) MW horn-antenna/parabolic reflector, 25 dBi antenna gain. (source: Fig. 7 in [117])

Figure 16. Single IMPACT FT-MW broadband spectrum of vitamin C after averaging of 9000 ps-LASER-ablation-gas pulses at 2 Hz repetition rate. The moleculare signals can unambiguously assigned to three different rotamers. The insert demonstrates the sub-Doppler resolution at the $J_{Ka,Kc} = 6_{0,6} \leftarrow 5_{0,5}$ rotational transition of conformer II. (source: Fig. 3 in [123])

Figure 17. The nine lowest-energy conformers of vitamin C (< 700cm^{-1} @ MP2/6-311++G(d,p)); five internal axes allow for differentr non-planar, three-dimensional cooperative hydrogen-bond networks, which include keto- and ether- besides hydroxyl-functions. Of a total of eleven possible, different intra-molecular hydrogen-bonds: $(n_a, n_b, n_c, n_d)_x$, $n_g = 1 \ldots 11$ labels the H-bonds, the index x distinguishes conformers with identical H-bond network. (source: Fig. 1 in [123] y)

Tables:

Table I. Approximate Extension of the Microwave Region

Range	Wavelength / cm	Wavenumber / cm^{-1}	Frequency / GHz
cm wave	1.0 - 100.0	1.0 - 0.01	30.0 - 0.3
mm wave	0.1 - 1.0	10.0 - 1.0	300.0 - 30.0
sub-mm wave	0.01 - 0.1	100.0 - 10.0[a]	3000.0 - 300.0[b]

[a] also often referred to as part of the far infra-red (FIR) range.
[b] terms terahertz (THZ) range or T-rays are used in relation to generation with pulsed LASERs.

References:

[1] C. H. Townes, A. L. Schawlow, Microwave Spectroscopy, McGraw-Hill Dover Publications, New York, 1955.

[2] J. C. McGurk, H. Mäder, R. T. Hofmann, T. G. Schmalz, W. H. Flygare, J. Chem. Phys. 61 (1974) 3759.

[3] W. H. Flygare, T. G. Schmalz, Acc. Chem. Res. 9 (1976) 385.

[4] J. C. McGurk, T. G. Schmalz, W. H. Flygare, in: I. Prigogine, S. A. Rice (Eds.), Advances in Chemical Physics, Vol. XXV, Wiley, New York, 1974, p. 1.

[5] H. Mäder, J. Quant. Spectrosc. Radiat. Transfer 32 (1984) 129.

[6] R. L. Shoemaker, in: J. I. Steinfeld (Ed.), Laser and coherence spectroscopy, Plenum, New York, 1978, p. 197.

[7] J. Gripp, H. Mäder, H. Dreizler, J. L. Teffo, J. Mol. Spectrosc. 172 (1995) 430.

[8] A. Bauder, in: J. Durig (Ed.), Vibrational spectra and structure, Vol. 20, Elsevier, Amsterdam, 1993, p. 157.

[9] J. Ekkers, W. H. Flygare, Rev. Sci. Instrum. 47 (1976) 448.

[10] H. Dreizler, Ber. Bunsenges. Phys. Chem. 99 (1995) 1451.

[11] R. Schwarz, A. Guarnieri, J.-U. Grabow, J. Doose, Rev. Sci. Instrum. 63 (1992) 4108.

[12] G. Bestmann, H. Dreizler, Z. Naturforsch. 38a (1983) 452.

[13] B. Vogelsanger, A. Bauder, J. Chem. Phys. 92 (1990) 4101.

[14] W. Jäger, J. Haekel, U. Andresen, H. Mäder, Mol. Phys. 68 (1989) 1287.

[15] H. Harder, H.-W. Nicolaisen, H. Dreizler, H. Mäder, J. Mol. Spectrosc. 160 (1993) 244.

[16] T. J. Balle, E. J. Campbell, M. R. Keenan, W. H. Flygare, J. Chem. Phys. 71 (1979) 2723.

[17] T. J. Balle, W. H. Flygare, Rev. Sci. Instrum. 52 (1981) 33.

[18] R. D. Suenram. F. J. Lovas, G. T. Fraser, J. Z. Gillies, C. W. Gillies, M. Onda, J. Mol. Spectrosc. 137 (1989) 127.

[19] J.-U. Grabow, W. Stahl, Z. Naturforsch. 45a (1990) 1043.

[20] C. Chuang, C. J. Hawley, T. Emilsson, H. S. Gutowsky, Rev. Sci. Instrum. 61 (1990) 1629.

[21] U. Andresen, H. Dreizler, J.-U. Grabow, W. Stahl, Rev. Sci. Instrum. 61 (1990) 3694.

[22] J.-U. Grabow, W. Stahl. H. Dreizler, Rev. Sci. Instrum. 67 (1996) 4072.

[23] J.-U. Grabow, E. S. Palmer, M. C. McCarthy, P. Thaddeus, Rev. Sci. Instrum. 76 (2005) 093106.

[24] J.-U. Grabow, *Habilitationsschrift*, Hannover, 2004.

[25] V. Strom, H. Dreizler, D. Consalvo, J.-U. Grabow, I. Merke, Rev. Sci. Instrum., 67 (1996) 2714.

[26] K. C. Etchison, C. T. Dewberry, K. E. Kerr, D. W. Shoup, S. A. Cooke, J. Mol. Spectrosc. 242 (2007) 39.

[27] W. F. Kolbe, B. Leskovar, Rev.Sci.Intrum. 56 (1985) 97.

[28] E. J. Campbell, L. W. Buxton, T. J. Balle, M. R. Keenan, W. H. Flygare, J. Chem. Phys. 74 (1981) 829.

[29] R. E. Smalley, L. Wharton, D. H. Levy, Acc. Chem. Res. 10 (1977) 139.

[30] R. R. Bousquet, P. M. Chu, R. S. DaBell, J.-U. Grabow, R. D. Suenram, IEEE Sensors J. 5 (2005) 656.

[31] R. D. Suenram, F. J. Lovas, G. T. Fraser, K. Matsumura, J. Chem. Phys. 92 (1990) 4724.

[32] K. A. Walker, M. C. L. Gerry, J. Mol. Spectrosc. 182 (1993) 178.

[33] J.-U. Grabow, N. Heineking, W. Stahl, Z. Naturforsch. 46a (1991) 914.

[34] Y. Endo, Y Oshima, J. Chem. Phys. 98 (1993) 6618.

[35] L. Bizzocchi, B. M. Giulinao, M. Hess, J.-U. Grabow, J. Chem. Phys. 126 (2007) 114305.

[36] F. J. Lovas, R. J. McMahon, J.-U. Grabow, M. Schnell, J. Mack, L. T. Scott, R. L. Kuczkowski, J. Am. Chem. Soc. 127 (2005) 4345.

[37] H. Hopf, C. Mlynek, R. J. McMahon, J. L. Menke, A. Lesarri, M. Rosemeyer, J.-U. Grabow, Chem. - Eur. J. 16 (2010) 14115.

[38] D. McNaughton, P. D. Godfrey, R. D. Brown, S. Thorwirth, J.-U. Grabow, Ap. J. 678 (2008) 309.

[39] D. McNaughton, P. Godfrey, M. K. Jahn, D. Dewald, J.-U. Grabow, J. Chem. Phys. 134, (2011) 154305.

[40] D. McNaughton, P. Godfrey, J.-U. Grabow, J. Mol. Spectrosc. 274, (2012) 1.

[41] F. J. Lovas, Y. Kawashima, J.-U. Grabow, R. D. Suenram, G. T. Fraser, E. Hirota, Astrophys. J. Lett. 455 (1995) L201.

[42] E. J. Cocinero, A. Lesarri, J.-U. Grabow, J. C: Lopez, J. L. Alonso, ChemPhysChem 8 (2007) 599.

[43] D. Banser, M. Schnell, J.-U. Grabow, E. J. Cocinero, A. Lesarri, J. L. Alonso, Angew. Chem. Int. Ed. 44 (2005) 6311.

[44] D. Banser, M. Schnell, J.-U. Grabow, E. J. Cocinero, A. Lesarri, J. L. Alonso, J. Mol. Struct. 795 (2006) 163.

[45] L. Bizzocchi, B. M. Giulinano, J.-U. Grabow, J. Mol. Struct. 833, 175(2007).

[46] B. M. Giuliano, L. Bizzocchi, S. Cooke, D. Banser, M. Hess, J. Fritzsche, J.-U. Grabow, Phys. Chem. Chem. Phys. 10 (2008) 2078.

[47] B. M. Giuliano, L. Bizzocchi, J.-U. Grabow, J. Mol. Spectrosc. 251 (2008) 261.

[48] B. M. Giuliano, L. Bizzocchi, R. Sanchez, P. Villanueva, V. Cortijo, M. E. Sanz, J.-U. Grabow, J. Chem. Phys. 135 (2011) 084303.

[49] B. A. Timp, J. L. Doran, S. Iyer, J.-U. Grabow, K. R. Leopold, J. Mol. Spectrosc. 271 (2012) 20.

[50] M. J. Travers, W. Chen, J.-U. Grabow, M. C. McCarthy, P. Thaddeus, J. Mol. Spectrosc. 192 (1998) 12.

[51] C. J. Evans, A. Lessari, M. C. L. Gerry, J. Am. Chem. Soc. 122 (2000) 6100.

[52] E. J. Cocinero, A. Lesarri, P. Écija, F. Basterretxea, J.-U. Grabow, J. A. Fernández, F. Castaño, Angew. Chem. Int. Ed. 51 (2012) 3119.

[53] N. Hansen, U. Andresen, H. Dreizler, J.-U. Grabow, H. Mäder, F. Temps, Chem. Phys. Lett. 289 (1998) 311.

[54] C. W. Gillies, J. Z. Gillies, R. D. Suenram, F. J. Lovas, E. Kraka, D. Cremer, J. Am. Chem. Soc. 113 (1991) 2412.

[55] J.-U. Grabow, A. M. Andrews, G. T. Fraser, K. K. Irikura, R. D. Suenram, F. J. Lovas, W. J. Lafferty, J. L. Domenech, J. Chem. Phys. 105 (1996) 7249.

[56] E.J. Goodwin, N.W. Howard, A.C. Legon, Chem. Phys. Lett. 131 (1986) 319.

[57] W. Caminati, J. C. Lopez, J. L. Alonso, J.-U. Grabow, Angew. Chem. Int. Ed. 44 (2005) 3840.

[58] G L. H. Coudert, W. Caminati, M. Schnell, J.-U. Grabow, J. Mol. Spectrosc. 242 (2007) 118.

[59] G. Feng, L. Evangelisti, L. B. Favero, J.-U. Grabow, Z. Xia, W. Caminati, Phys. Chem. Chem. Phys. 13 (2011) 14092.

[60] J. L. Alonso, E. J. Cocinero, A. Lesarri, M. E. Sanz, J. C. Lopez, Angew. Chem. Int. Ed. 45 (2006) 3471.

[61] H.-W. Nicolaisen, J.-U. Grabow, N. Heineking, W. Stahl, Z. Naturforsch. 462 (1991) 635.

[62] M. Meyer, J.-U. Grabow, H. Dreizler, J. Mol. Spectrosc. 151 (1992) 217.

[63] J.-U. Grabow, N. Heineking, W. Stahl, J. Mol. Spectrosc.154 (1992) 129.

[64] J. L. Alonso, A. Lesarri, S. Mata, J. C. Lopez, J.-U. Grabow, H. Dreizler, Chem. Phys. 208 (1996) 391.

[65] J. Z. Gillies, C. W. Gillies, J.-U. Grabow, H. Hartwig, E. Block, J. Phys. Chem. 100 (1996) 18708.

[66] J.-U. Grabow, H. Hartwig, N. Heineking, W. Jäger, H. Mäder, H.-W. Nicolaisen, W. Stahl, J. Mol. Struct. 612 (2002) 349.

[67] I. Merke, W. Stahl, S. Kassi, D. Petitprez, G. Wlodarczak, J. Mol. Spectr. 216 (2002) 437.

[68] M. Schell, J.-U. Grabow, H. Hartwig, N. Heineking, M. Meyer, W. Stahl, W. Caminati, J. Mol. Spectrosc. 229 (2005) 1.

[69] W. Caminati, S. Melandri, M. Schnell, D. Banser, J.-U. Grabow, J. L. Alonso, J. Mol. Struct. 742 (2005) 87.

[70] W. Caminati, J.-U. Grabow, J. Am. Chem. Soc. 128 (2006) 854.

[71] L. Evangelisti, A. Lesarri, M. K. Jahn, E. Cocinero, W. Caminati, J.-U. Grabow, J. Phys. Chem. A 115 (2011) 9545.

[72] M. Schnell, J.-U. Grabow, Phys. Chem. Chem. Phys. 8 (2006) 2209.

[73] M. Schnell, J.-U. Grabow, Angw. Chem. Int. Ed. 45 (2006) 3465.

[74] M. Schnell, J.-U. Grabow, Chem. Phys. 343 (2008) 121.

[75] M. Schnell, J. T. Hougen, J.-U. Grabow, J. Mol. Spectrosc. 251 (2008) 38.

[76] L. Favero, W. Caminati, J.-U. Grabow, J. Mol. Spectrosc. 255 (2009) 199.

[77] V. V. Ilyushin, L. B. Favero, W. Caminati, J.-U. Grabow, ChemPhysChem. 11 (2010) 2589.

[78] L. B. Favero, J.-U. Grabow, W. Caminati, Chem. - Eur. J. 18 (2012) 2468.

[79] B. M. Giuliano, P. Ottaviani, L. B. Favero, W. Caminati, J.-U. Grabow, A. Giardini, M. Satta, Phys. Chem. Chem. Phys. 9 (2007) 4460.

[80] A. Lesarri, J.-U. Grabow, W. Caminati, Chem. Phys. Lett. 468 (2009) 18.

[81] E. J. Cocinero, A. Lesarri, P. Ecija, J.-U. Grabow, J. A. Fernandez, F. Castano, Phys. Chem. Chem. Phys. 12 (2010) 6067.

[82] A. Lesarri, E. J. Cocinero, L. Evangelisti, R. D. Suenram, W. Caminati, J.-U. Grabow, Chem. - Eur. J. 16 (2010) 10214.

[83] E. J. Cocinero, A. Lesarri, P. Écija, J.-U. Grabow, J. A. Fernández, F. Castaño, Phys. Chem. Chem. Phys. 12 (2010) 12486.

[84] A. Lesarri, A. Vega-Toribio, R. D. Suenram, D. J. Brugh, J.-U. Grabow, Phys. Chem. Chem. Phys. 12 (2010) 9624.

[85] A. Lesarri, A. Vega-Toribio, R. D. Suenram, D. J. Brugh, D. Nori-Shargh, J. E. Boggs, J.-U. Grabow, Phys. Chem. Chem. Phys. 13 (2011) 6610.

[86] M. Rudrum, D. F. Shaw, J. Chem. Soc. (1965) 52.

[87] R. U. Lemieux, J. D. Stevens, Can. J. Chem. 44 (1966) 249.

[88] E. Breitmaier, U. Hollstein, Org. Magn. Reson. 8 (1976) 573.

[89] J.-P. Schermann, *Spectroscopy and Modelling of Biomolecular Building Blocks*, Elsevier, Amsterdam, 2008.

[90] N. Vogt, K. P. R. Nair, J. Vogt, J.-U. Grabow, J. Mol. Spectrosc. 268 (2011) 16.

[91] J. Demaison, N. C. Craig, E. J. Cocinero, J.-U. Grabow, A. Lesarri, H. D. Rudolph, J. Phys. Chem. A 116 (2012) 8684.

[92] J.-U. Grabow, A. S: Pine, G. T. Fraser, F. J. Lovas, R. D. Suenram, T. Emilsson, E. Arunan, H. S: Gutowsky, J. Chem. Phys. 102 (1995) 1181.

[93] Y. Xu, W. Jäger, J. Chem. Phys. 107 (1997) 4788.

[94] J. Tang, Y. Xu, A. R. W. McKellar, W.Jäger, Science 297 (2002) 2030.

[95] E. J. Campbell, W. G. Read J. A. Shea, Chem. Phys. Lett. 94 (1983) 69.

[96] D. Consalvo, Rev. Sci. Instrum. 69 (1998) 3136.

[97] T. Emilsson, H. S. Gutowsky, G. De Oliveira, C. E. Dykstra, J. Chem. Phys. 112 (2000) 1287.

[98] Z. Kisiel, J. Kosarzewski, B. A. Pietrewicz, L. Pszczolkowski, Chem. Phys. Lett. 325 (2000) 523.

[99] M. Schnell, D. Banser, J.-U. Grabow, Rev. Sci. Instrum. 75 (2004) 2111.

[100] K. Wohlfahrt, M. Schnell, J.-U. Grabow, J. Küpper, J. Mol. Spectrosc. 247 (2008) 119.

[101] F. Filsinger, K. Wohlfahrt, M. Schnell, J.-U. Grabow, J. Küpper, Phys. Chem. Chem. Phys. 10 (2008) 666.

[102] H. S. P. Müller, A. Coutens, A. Walters, J.-U. Grabow, S. Schlemmer, J. Mol. Spectrosc. 267 (2011) 100.

[103] K.K. Baldridge, J.S. Siegel, Theor. Chem. Acc. **97**, 67-71 (1997).

[104] J. Baron, W. C. Campbell, D. DeMille, J. M. Doyle, G. Gabrielse, Y. V. Gurevich, P. W. Hess, N. R. Hutzler, E. Kirilov, I. Kozyryev, B. R. O'Leary, C. D. Panda, E. S. Petrik, B. Spaun, A. C. Vutha, A. D. West. Science 1248213 (2013).

[105] L. D. Alphei, J.-U. Grabow, A. N. Petrov, R. Mawhorter, B. Murphy, A. Baum, T. J. Sears, T. Zh.Yang, P.M Rupasinghe, C. P. McRaven, N. E. Shafer-Ray, Phys. Rev. A 83 (2011) 040501R.

[106] R. Mawhorter, B. Murphy, A. Baum, T. J. Sears, T. Zh.Yang, P.M Rupasinghe, C. P. McRaven, N. E. Shafer-Ray, L. D. Alphei, J.-U. Grabow, Phys. Rev. A 84 (2011) 022508.

[107] J. Hudson, B. Sauer, M. Tarbutt, and E. Hinds, Phys. Rev. Lett. 89 (2002) 23003.

[108] R. R. Ernst, W. A. Anderson, Rev. Sci. Instrum. 37 (1966) 93.

[109] J. C. McGurk, T. G. Schmalz, W. H. Flygare, J. Chem. Phys. 60 (1974) 4181.

[110] M. K. Jahn, D. Wachsmuth, D. A. Dewald, J.-U. Grabow, S. C. Mehrotra, J. Mol. Spectrosc. 280 (2012) 54.

[111] F. Wolf, J. Phys. D Appl. Phys. 27 (1994) 1774.

[112] V. V. Khodos, D. A. Ryndyk, V. L. Vaks, Eur. Phys. J. Appl. Phys. 25 (2004) 203.

[113] G.G. Brown, B. C. Dian, K. O. Douglass, S. M. Geyer, B. H. Pate, J. Mol. Spectrosc. 238 (2006) 200.

[114] G. S. Grubbs II, C. T. Dewberry, K. C. Etchison, K. E. Kerr, S. A. Cooke, Rev. Sci. Instrum. 78 (2007) 096106.

[115] J.-U. Grabow, ChemPhysChem, in Vorbereitung, 2013.

[116] J.-U. Grabow, S. Mata, J. L. Alonso, I. Peña, S. Blanco, J. C. Lopez, C. Cabezas, Phys. Chem. Chem. Phys. 13 (2011) 21063.

[117] J.-U. Grabow, *Applikationsschrift*, 2. Aufl., in Vorbereitung, Hannover 2013.

[118] *Special Issue: Broadband Rotational Spectroscopy*, B. H. Pate, F. C. De Lucia (eds.), J. Mol. Spectrosc. 280 (2012).

[119] C. Perez, M. T. Muckle, D. P. Zaleski, N. A. Seifert, B. Temelso, G. C. Shields, Z. Kisiel, B. H. Pate, Science 336 (2012) 897.

[120] B. C. Dian, G. G. Brown K. O. Douglass, B. H. Pate, Science 320 (2008) 924.

[121] S.Katsumata, N. Ikehata, J. Electron Spectrosc. Relat. Phenom. 107 (2000) 139.

[122] I. Novak, A. W. Potts, Biochim. Biophys. Acta, Bioenerg., 1319 (1997) 86.

[123] I. Peña, A. M. Daly, C. Cabezas, S. Mata, C. Bermúdez, A. Niño, J. C. Lopez, J.-U. Grabow, and J. L. Alonso, J. Phys. Chem. Lett. 4 (2013) 65.

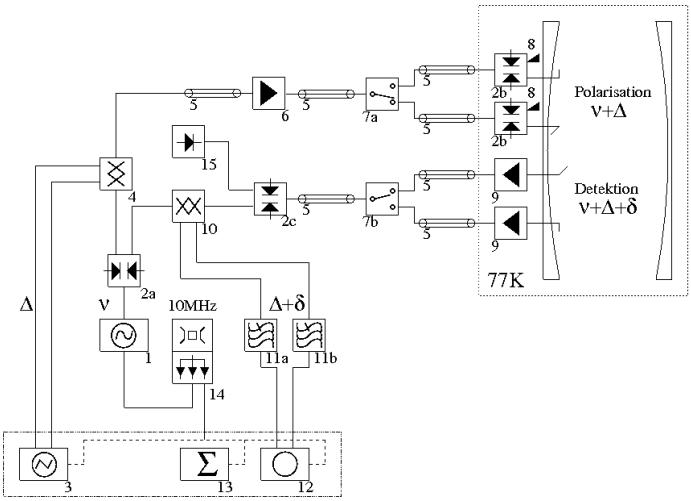

Fig. 1

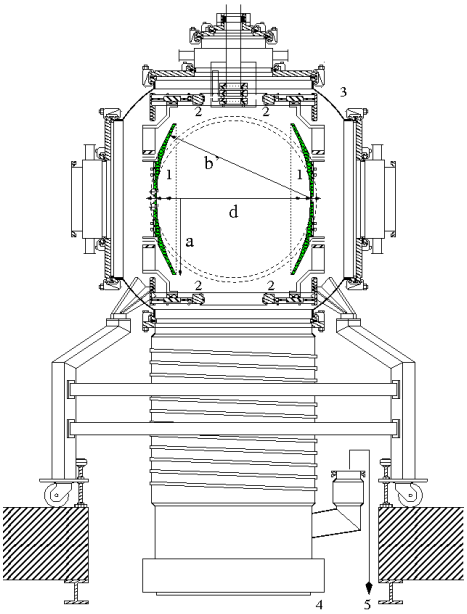

Fig. 2

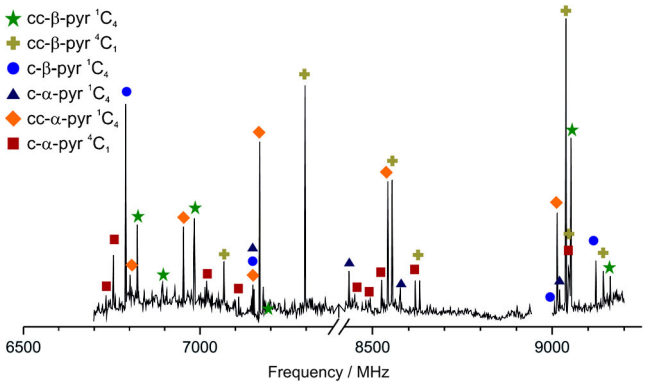

Fig. 3

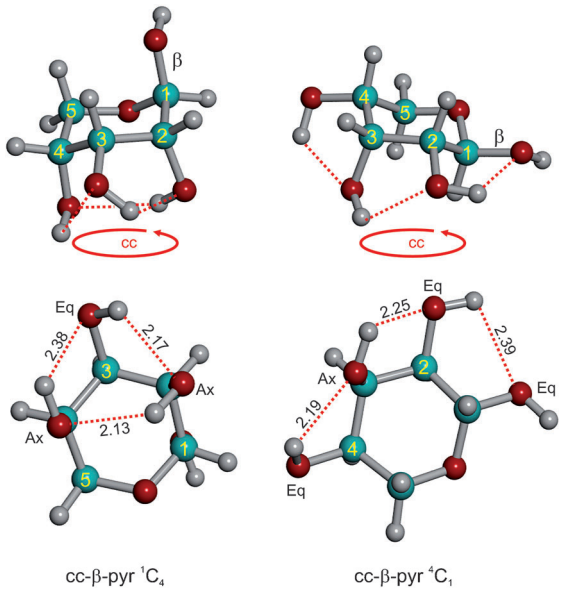

Fig. 4

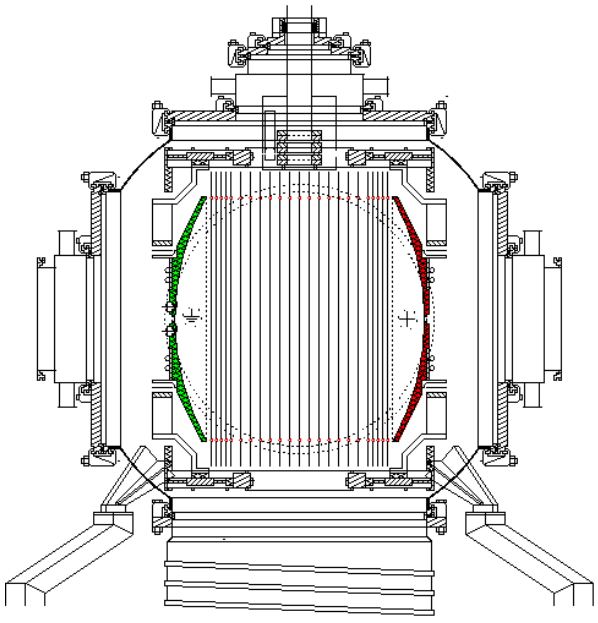

Fig. 5

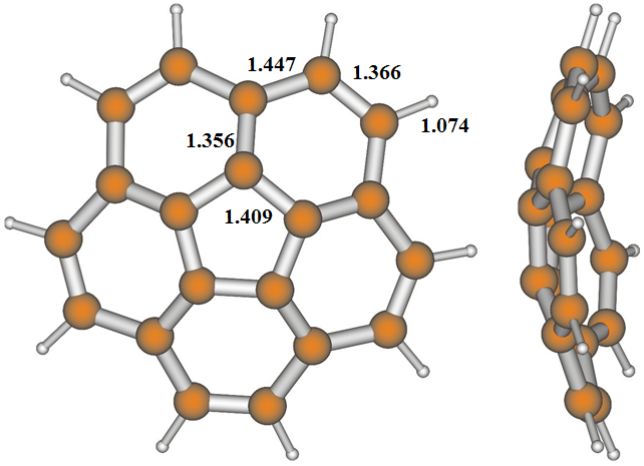

Fig. 6

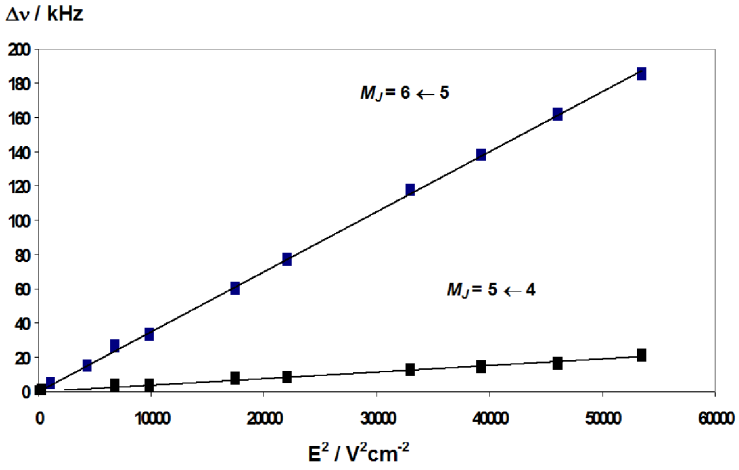

Fig. 7

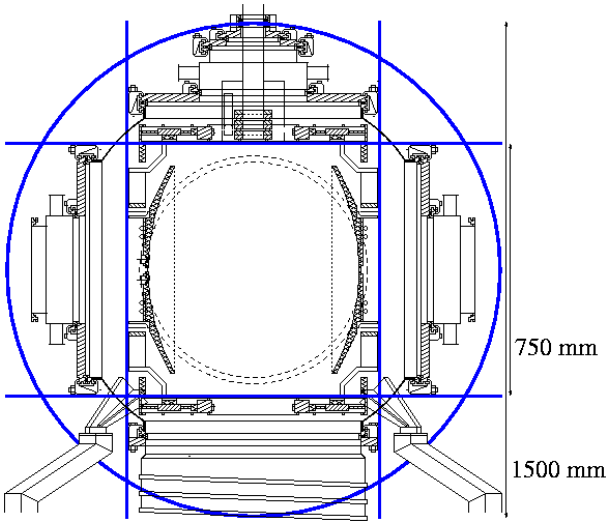

Fig. 8

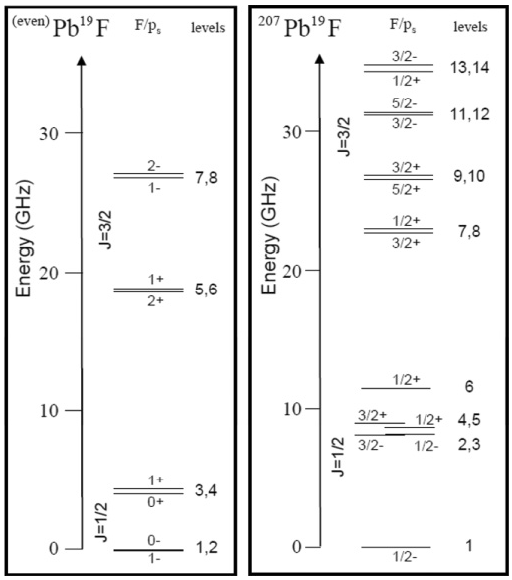

Fig. 9

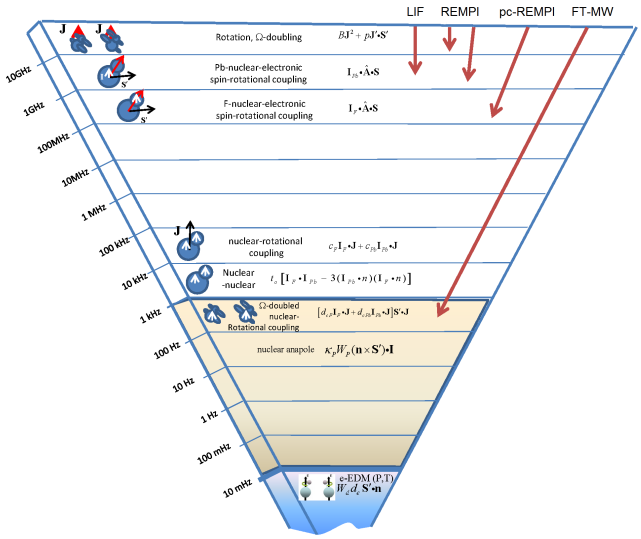

Fig. 10

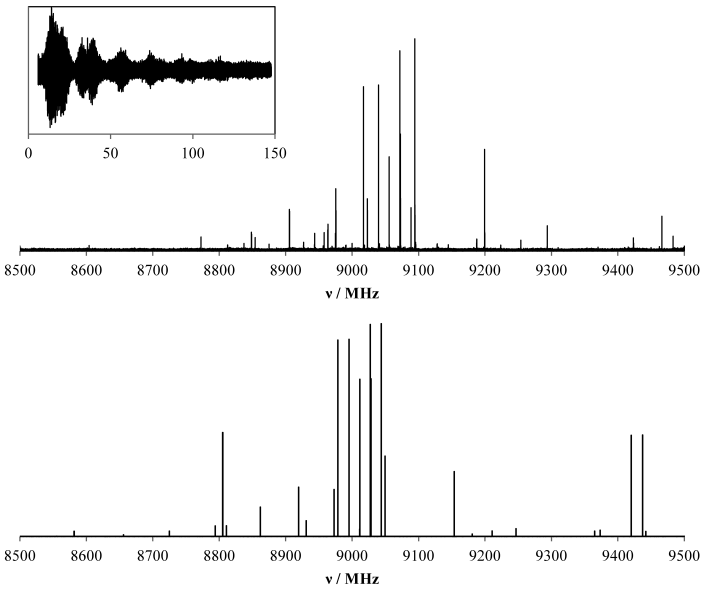

Fig. 11

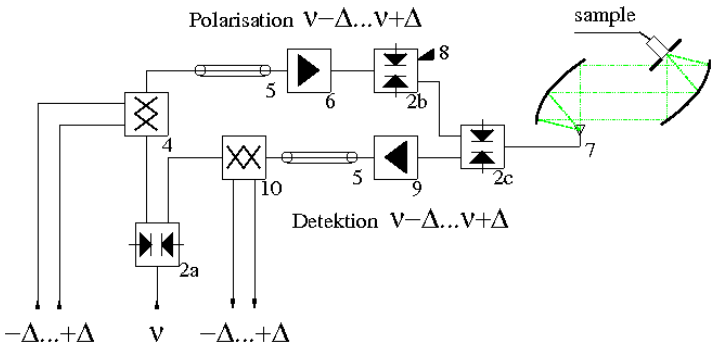

Fig. 12

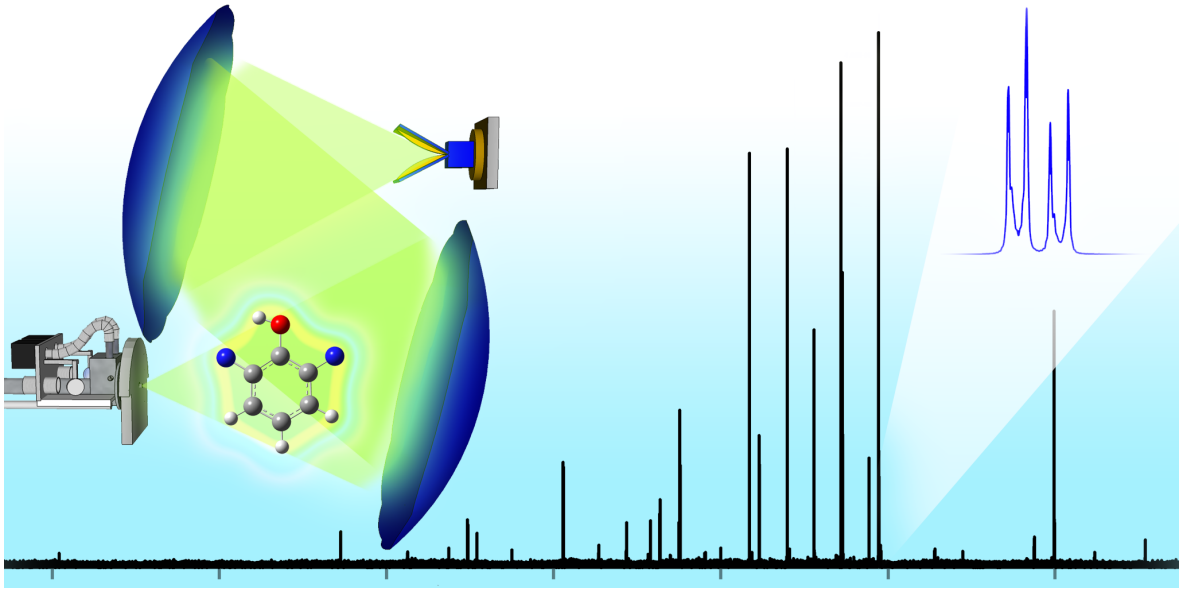

Fig. 13

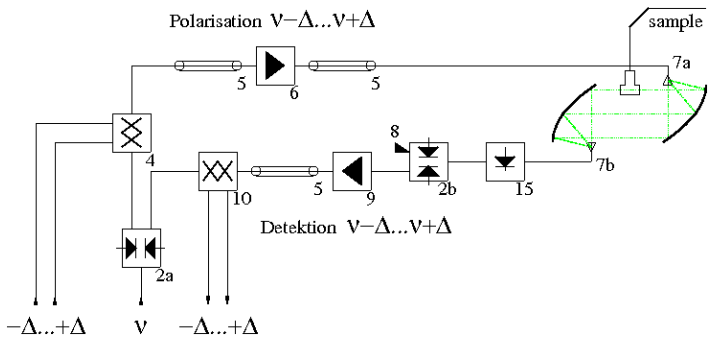

Fig. 14

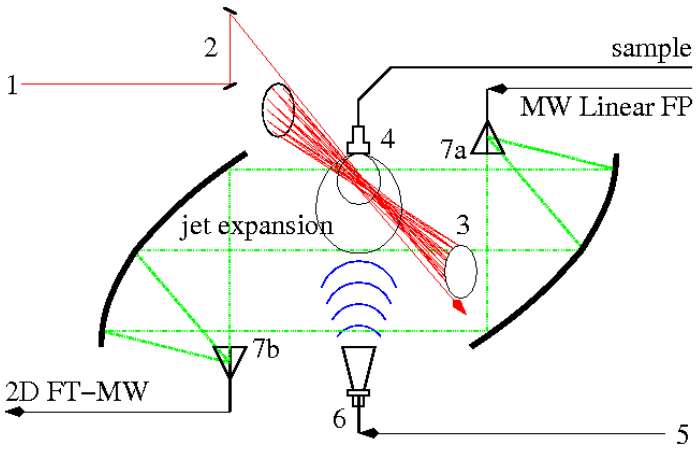

Fig. 15

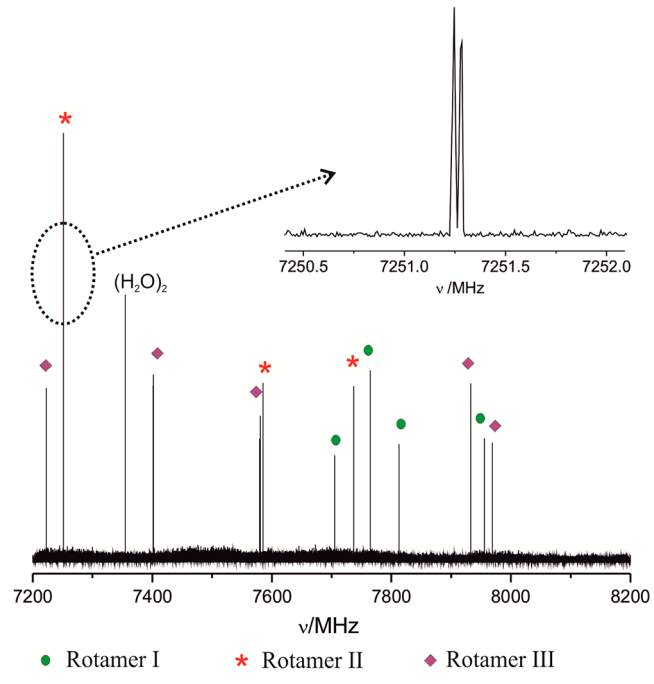

Fig. 16

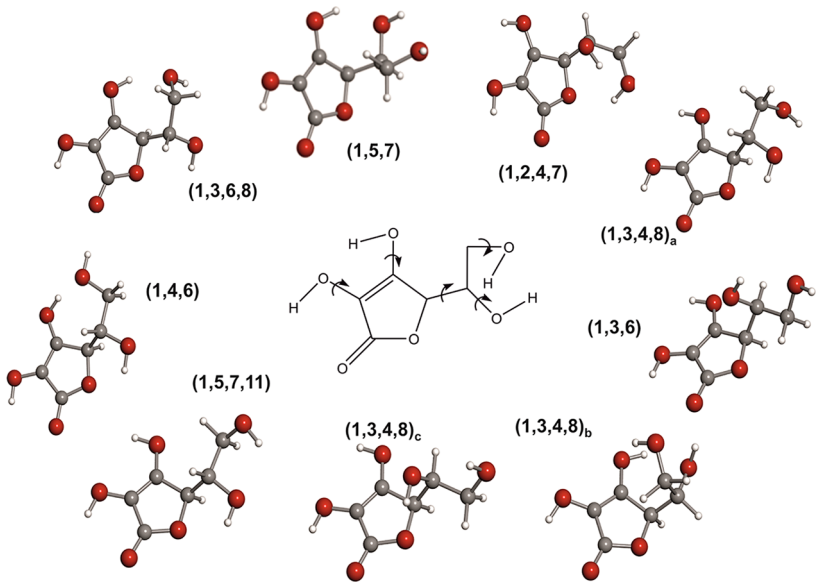

Fig. 17